Cargo-selective SNX-BAR proteins mediate retromer trimer independent retrograde transport

Arunas Kvainickas,[1,2] Ana Jimenez-Orgaz,[1,2] Heike Nägele,[1] Zehan Hu,[3] Jörn Dengjel,[3] and Florian Steinberg[1]

[1]Center for Biological Systems Analysis and [2]Faculty of Biology, Albert Ludwigs Universitaet Freiburg, Freiburg, Germany
[3]Department of Biology, Fribourg University, Fribourg, Switzerland

The retromer complex, which recycles the cation-independent mannose 6-phosphate receptor (CI-MPR) from endosomes to the trans-Golgi network (TGN), is thought to consist of a cargo-selective VPS26–VPS29–VPS35 trimer and a membrane-deforming subunit of sorting nexin (SNX)–Bin, Amphyphysin, and Rvs (BAR; SNX-BAR) proteins. In this study, we demonstrate that heterodimers of the SNX-BAR proteins, SNX1, SNX2, SNX5, and SNX6, are the cargo-selective elements that mediate the retrograde transport of CI-MPR from endosomes to the TGN independently of the core retromer trimer. Using quantitative proteomics, we also identify the IGF1R, among more potential cargo, as another SNX5 and SNX6 binding receptor that recycles through SNX-BAR heterodimers, but not via the retromer trimer, in a ligand- and activation-dependent manner. Overall, our data redefine the mechanics of retromer-based sorting and call into question whether retromer indeed functions as a complex of SNX-BAR proteins and the VPS26–VPS29–VPS35 trimer.

Introduction

The retromer complex is an ancient highly conserved multiprotein complex that orchestrates the recycling of a wide range of internalized transmembrane proteins from early and maturing endosomes either to the trans-Golgi network (TGN) or back to the plasma membrane (Burd and Cullen, 2014). Retromer is thought to consist of a constitutive trimer of VPS26, VPS29, and VPS35 as well as a more loosely associated set of sorting nexins (SNXs) with a Bin, Amphiphysin, and Rvs (BAR) domain, namely SNX1, SNX2, SNX5, and SNX6 (Seaman et al., 1998; Griffin et al., 2005; Shi et al., 2006; Hierro et al., 2007; Rojas et al., 2007; Wassmer et al., 2007). The vacuolar protein-sorting (VPS) trimer associates with endosomal membranes through an interaction with the small GTPase RAB7 and SNX3 and is often described as the cargo-selective complex because of its reported affinity for some of the cargoes that it recycles (Seaman, 2004, 2007; Strochlic et al., 2007; Seaman et al., 2009; Fjorback et al., 2012; Harrison et al., 2014; Lucas et al., 2016). Besides engaging the Ankyrin-repeat protein ANKRD50, which is necessary for retromer function (Kvainickas et al., 2017), the retromer trimer also recruits the actin-polymerizing Wiskott-Aldrich syndrome protein and SCAR homologue (WASH) complex, which generates branched actin networks on the endosomal surface (Derivery et al., 2009; Gomez and Billadeau, 2009). The retromer SNX-BAR proteins form heterodimers of SNX1 or SNX2 with SNX5 or SNX6 (Wassmer et al., 2007; van Weering et al., 2012), bind to phosphatidyl-inositol-3-phopshate (PI3P) on the endosomal surface, and can potentially detect membrane curvature through their BAR domain and may be able to tubulate the endosomal membrane when local concentration is high enough (Carlton et al., 2004). The current working model of the retromer is: The RAB7- and SNX3-bound core VPS trimer generates an actin-decorated endosomal subdomain that attracts, traps, and enriches cargo through direct binding to the VPS trimer, followed by formation of a cargo-enriched tubular carrier that is formed through a helical array of SNX-BARs and the VPS trimer (Gallon and Cullen, 2015). Nonsynonymous point mutations in the core retromer subunit VPS35 have recently been shown to cause hereditary Parkinson's disease (Vilariño-Güell et al., 2011; Zimprich et al., 2011), which makes a thorough mechanistic understanding of retromer-based sorting important from a medical perspective. Most of the mechanistic insight on the retromer complex was gained from studying its role in the retrograde transport of the cation-independent mannose 6-phosphate receptor (CI-MPR; also known as IGF2R), which delivers lysosomal hydrolases through cycling between the TGN and early/late endosomes, from which it is assumed to be recycled back to the TGN through direct binding of the CI-MPR tail to the VPS trimer (Arighi et al., 2004; Seaman, 2004). In this study, we fundamentally question the current model of how retromer operates as the core VPS trimer is not required for the retrograde transport of the CI-MPR. Instead,

Correspondence to Florian Steinberg: florian.steinberg@zbsa.de

Abbreviations used: BAR, Bin, Amphiphysin, and Rvs; CI-MPR, cation-independent mannose 6-phosphate receptor; gRNA, guide RNA; INSR, insulin receptor; IP, immunoprecipitation; KO, knockout; LC-MS/MS, liquid chromatography–tandem mass spectrometry; PX, Phox homology; SILAC, stable isotope labeling with amino acids in cell culture; SNX, sorting nexin; STED, stimulated emission depletion; TALEN, transcription activator-like effector nuclease; TGN, trans-Golgi network; VPS, vacuolar protein-sorting.

© 2017 Kvainickas et al. This article is distributed under the terms of an Attribution–Noncommercial–Share Alike–No Mirror Sites license for the first six months after the publication date (see http://www.rupress.org/terms/). After six months it is available under a Creative Commons License (Attribution–Noncommercial–Share Alike 4.0 International license, as described at https://creativecommons.org/licenses/by-nc-sa/4.0/).

The Rockefeller University Press
J. Cell Biol. Vol. 216 No. 11 3677–3693
https://doi.org/10.1083/jcb.201702137

THE JOURNAL OF CELL BIOLOGY

Downloaded from http://rupress.org/jcb/article-pdf/216/11/3677/1374505/jcb_201702137.pdf by guest on 26 August 2022

we demonstrate that the SNX-BAR proteins are cargo selective for CI-MPR and other cargo and function independently of the core retromer trimer.

Results

The core retromer trimer is not required for retrograde sorting of CI-MPR

Throughout our studies of the retromer complex, we had difficulties replicating the previously described retrograde sorting defects of the CI-MPR in VPS trimer–depleted cells, which are described as a pronounced dispersal of the CI-MPR from its natural steady-state localization at the TGN to early endosomes because of a defect in recycling from these endosomes back to the TGN (Arighi et al., 2004; Seaman, 2004; Hao et al., 2013). This defect in recycling was also reported to result in lysosomal missorting of CI-MPR and subsequent degradation (Arighi et al., 2004; Seaman, 2007). One possible explanation for our inability to replicate the CI-MPR sorting defects may have been because of unspecific reagents for the visualization of CI-MPR. Knockout (KO) of CI-MPR in human HAP1 and HeLa cells, however, led to a complete loss of immunofluorescent and Western blot signal for the two monoclonal CI-MPR antibodies used in this study (Fig. S1, A–C), indicating full specificity. Because insufficient suppression of retromer through RNAi could also be a cause for the lack of effects, we used CRISPR-Cas9 as well as transcription activator-like effector nuclease (TAL EN)-mediated gene targeting to genomically delete the core retromer subunit VPS35 from human HeLa and U2OS cells. CRISPR-Cas9–mediated disruption of exon 5 or exon 8 of the VPS35 gene in HeLa cells resulted in a loss of all VPS trimer components (Fig. 1 A). Retromer function was also disrupted as the established retromer cargo GLUT1 (Steinberg et al., 2013) was lost from the cell surface as a result of fully penetrant lysosomal missorting (Fig. 1 A). Lentiviral reexpression of HA-tagged VPS35 restored vesicular VPS35 expression and reverted the GLUT1 phenotype (Fig. S1 D), thereby ruling out off-target damage to the recycling machinery in the KO clones. All tested clonal VPS35-KO cell lines had total and cell surface levels of CI-MPR that were roughly equal to parental HeLa cells (Fig. 1 A). Strikingly, these cells did not display any retrograde sorting defects as the steady-state distribution of CI-MPR remained unchanged at the TGN46-labeled TGN (Fig. 1 B). All tested HeLa VPS35-KO cell lines had a pronounced GLUT1 phenotype (Fig. S2 A) but displayed no evidence of CI-MPR dispersal from the TGN (Fig. S2 B) or early endosomal accumulation of CI-MPR (Fig. S2 C). Dynamic uptake assays with a mAb targeting the extracellular domain of the endogenous CI-MPR showed that the internalized antibody–CI-MPR complex even reached the TGN slightly faster than in parental HeLa cells over 30 and 60 min, again arguing against a sorting defect from endosomes to the TGN (Fig. 1 C). Genomic deletion of CI-MPR in HeLa cells completely abolished antibody uptake, ruling out unspecific binding or fluid phase uptake of the antibody (Fig. S2 D). In agreement with the normal steady-state levels of total CI-MPR, we failed to detect lysosomal missorting (Fig. 1 D, right) or enhanced degradation rates of the receptor in cells treated with the ribosomal inhibitor cycloheximide (Fig. 1 D). As disruption of VPS35 resulted in no measurable retrograde sorting defect of CI-MPR, we also used CRISPR-Cas9 to disrupt the core retromer subunit VPS29 in HeLa cells. Loss of VPS29 resulted in a pronounced loss of endogenous VPS35 (∼75%) and VPS26 (∼90%) but did not lead to lower levels of CI-MPR (Fig. 2 A) in several tested clonal KO cell lines. The retromer cargo GLUT1 was severely lost from the surface of the VPS29-KO cells and accumulated in lysosomes, indicating a complete loss of retromer function (Fig. 2 B). Lentiviral reexpression of VPS29 fully restored cell surface GLUT1, ruling out off-target effects of the VPS29 deletion. In contrast with the obvious GLUT1 missorting, localization of CI-MPR to the TGN was comparable to parental HeLa cells (Fig. 2 D).

Similarly, disruption of VPS35 with TALENs targeting exon 4 in the frequently used U2OS osteosarcoma cell line (clone information is shown in Fig. S1 E) also led to a complete loss of the VPS35 protein (Fig. 3 A) but did not result in lower levels of the CI-MPR (Fig. 3 A) nor in any dispersal from the TGN (Fig. 3 B) or instability of the CI-MPR (Fig. 3 C) in the clonal KO cell lines. In addition, we also disrupted the VPS35 gene through CRISPR-Cas9 targeting in human SHSY5Y and MDA–MB-231 cells but could not detect any changes in CI-MPR distribution (Fig. S2, E and F). To exclude that long-term adaption to the loss of VPS35 obscured the CI-MPR sorting defects, we also used highly efficient siRNA against VPS35 to acutely deplete it from HeLa cells. Knockdown of VPS35 resulted in a virtually complete loss of VPS35 in Western blots (Fig. 3 D) and a fully penetrant GLUT1 phenotype (Fig. 3 D). In contrast, we could not detect any effect on TGN localization of CI-MPR and also detected no increase in lysosomal localization (Fig. 3 E). Similarly, efficient knockdown of VPS35 in U2OS cells failed to cause visible changes in CI-MPR levels and distribution (Fig. S2 F). We concluded that the core retromer trimer is not required for the retrograde sorting of CI-MPR to the TGN.

SNX-BAR proteins are the retrograde carrier for CI-MPR

To identify the retrograde sorting mechanism of CI-MPR in an unbiased way, we performed stable isotope labeling with amino acids in cell culture (SILAC)-based quantitative proteomics of the GFP-tagged isolated CI-MPR tail, which was lentivirally transduced into HEK293 cells with GFP alone as the paired control (Fig. 4 A). Interestingly, the GFP-tagged cytosolic tail localized to a perinuclear structure resembling the Golgi stack (Fig. 4 A, left). GFP-trap isolation of GFP from unlabeled cells and GFP–CI-MPR tail from heavy isotope–labeled cells followed by liquid chromatography–tandem mass spectrometry (LC-MS/MS)–based quantification of the pooled samples revealed robust interactions with previously published interactors such as the Golgi-localized GGA1 and GGA2 proteins as well as AP-1 complex components (Ghosh et al., 2003), which likely explains the apparent localization of the tail construct to Golgi membranes. Unexpectedly, all four retromer-associated SNX-BAR proteins (SNX1, SNX2, SNX5, and SNX6) as well as SNX27 were also heavily enriched with the tail (Fig. 4 A and Table S1). Western blotting of GFP trap–isolated CI-MPR tail immunoprecipitations (IPs) confirmed association of the endogenous SNX-BARs and SNX27 with the CI-MPR tail, whereas VPS35 was absent in the precipitates (Fig. 4 B). GFP-trap precipitation of the GFP-tagged SNXs showed that SNX5, SNX6, and also the SNX6 homologue SNX32 (but not VPS35) precipitated the endogenous CI-MPR efficiently, whereas SNX1 and SNX2 precipitated CI-MPR only slightly (2–3×) above the GFP-only background (Fig. 4 C). As the retrograde sorting motif in the tail had been mapped to a hydrophobic WLM

Downloaded from http://rupress.org/jcb/article-pdf/216/11/3677/1374505/jcb_201702137.pdf by guest on 26 August 2022

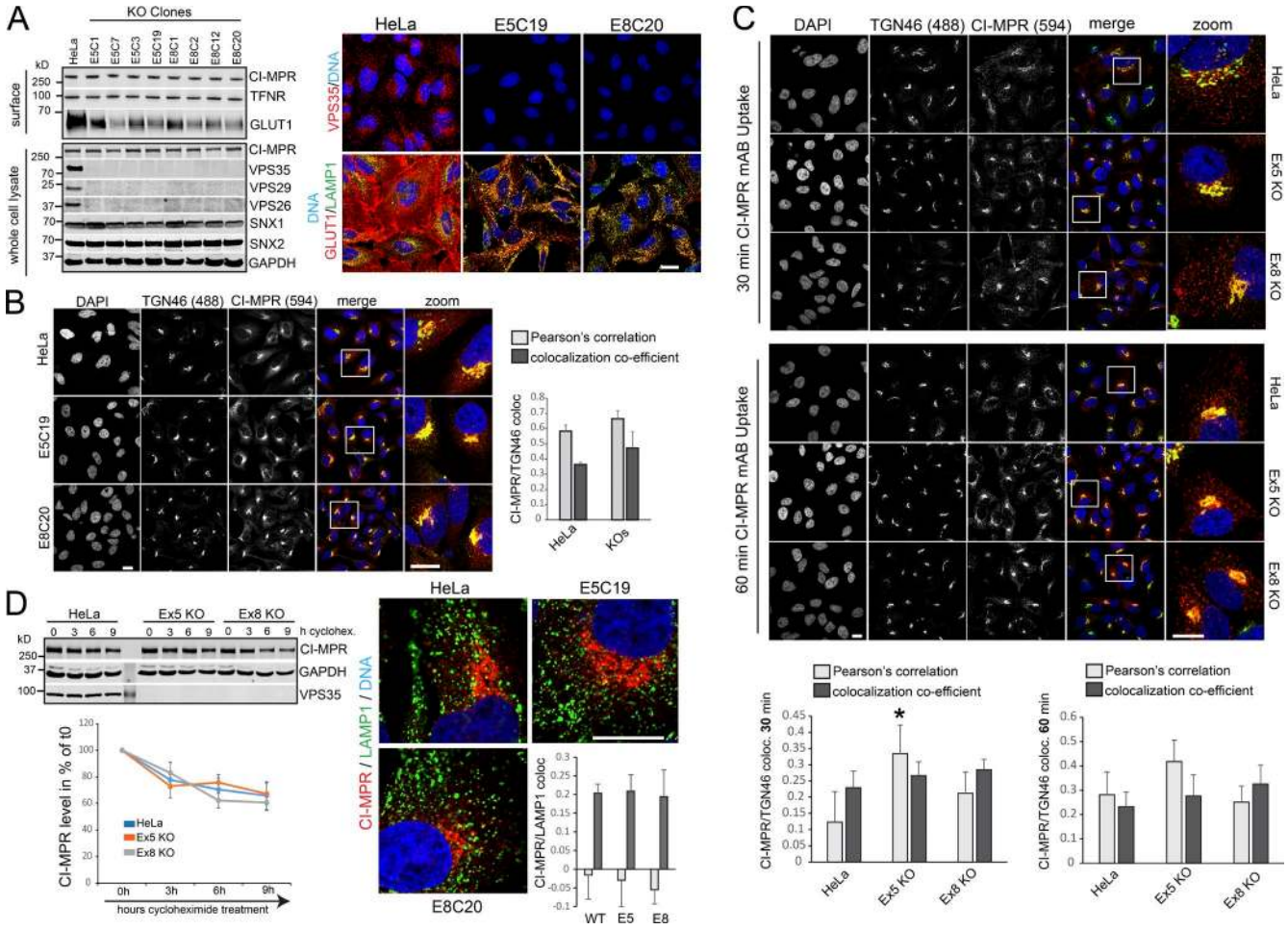

Figure 1. **Genomic deletion of VPS35 does not cause retrograde sorting defects of CI-MPR.** (A) Western blot of lysates from clonal HeLa cell lines with a disruption of the VPS35 gene in exon 5 or exon 8 (left). Immunofluorescent staining of endogenous GLUT1 (red) and endogenous LAMP1 (green) in HeLa cells and in two distinct VPS35-KO cell lines (right). (B) Staining of endogenous CI-MPR (red) and TGN46 (green) in parental HeLa cells and two VPS35-KO cell lines. The colocalization (coloc) between the TGN marker TGN46 and CI-MPR was quantified over three independent experiments. (C) Uptake assay with an antibody against the extracellular domain of CI-MPR in HeLa and VPS35-KO cell lines. Delivery of the CI-MPR–antibody complex (red) to the TGN46 (green)-labeled TGN was quantified after 30 and 60 min of uptake at 37°C over three independent experiments. (D) CI-MPR degradation assays in parental HeLa and VPS35-KO cells treated with the ribosomal inhibitor cycloheximide for indicated time points (left). Graph shows the degradation kinetics averaged over four independent experiments. Immunofluorescence of endogenous CI-MPR (red) and endogenous LAMP1 (green) in HeLa and VPS35-KO cell lines quantified over three independent experiments (right). Bars, 10 µm. Error bars indicate SD. *, $P < 0.05$ compared with control conditions in a *t* test.

(2,369–2,371 aa) motif previously described (Seaman, 2007), we next tested whether this motif is needed to engage the SNX-BAR proteins. Indeed, only the WLM motif–containing part (2,368–2,394 aa) precipitated the endogenous SNX-BARs, whereas the more C-terminal part and a WLM-AAA mutant did not (Fig. 4 D). Finally, we used recombinant His-tagged SNX-BARs produced as secreted proteins in HEK293 cells to test for direct interaction with the GST-tagged CI-MPR tail isolated from bacteria. SNX6-His failed to express, but SNX1-His, SNX2-His, and SNX5-His could be isolated as secreted proteins. When expressed and tested for interaction individually, all three failed to bind the CI-MPR tail (Fig. 4 E). Coexpression of His-tagged SNX1–SNX5 or SNX2–SNX6 dimers allowed production of SNX6 (Fig. 4 F). The WT CI-MPR tail efficiently bound dimers of either SNX1/5 or SNX2/6, whereas the WLM-AAA mutant version failed to do so (Fig. 4 F). It should be noted here that the SNX-BARs produced as secreted proteins in HEK293 cells were glycosylated as they displayed a higher apparent molecular weight than the endogenous proteins, which could be reduced partially by treatment with the glycosidase PNGaseF (Fig. S3 A). However, SNX1-His and SNX5-His produced in HEK293 cells treated with the glycosylation inhibitor tunicamycin displayed similar binding to the CI-MPR tail and also failed to efficiently bind to the WLM-AAA mutant tail (Fig. S3 B). We concluded that dimers of SNX1–SNX5 or SNX2–SNX6 can directly bind the CI-MPR tail, with SNX5 and SNX6 as the likely cargo-selective elements.

We next designed three distinct (targeting different genomic regions of the same gene) CRISPR-Cas9–based targeting vectors against most of the high-confidence interactors from our proteomics screen. Plasmids targeting RAB7A and clathrin heavy chain were added as a positive control as loss of these proteins should disrupt CI-MPR sorting. The three or six plasmids (for double targeting of SNX1/2 and SNX5/6) plasmids for each gene were pooled and transfected together with a puromycin resistance–expressing plasmid. After puromycin selection, sufficient targeting efficiency for all tested genes was confirmed by Western blotting (Fig. 4 G), which showed that all proteins were reduced in their expression to near-undetectable levels. The CRISPR-treated cells were then analyzed for a loss of CI-

Downloaded from http://rupress.org/jcb/article-pdf/216/11/3677/1374505/jcb_201702137.pdf by guest on 26 August 2022

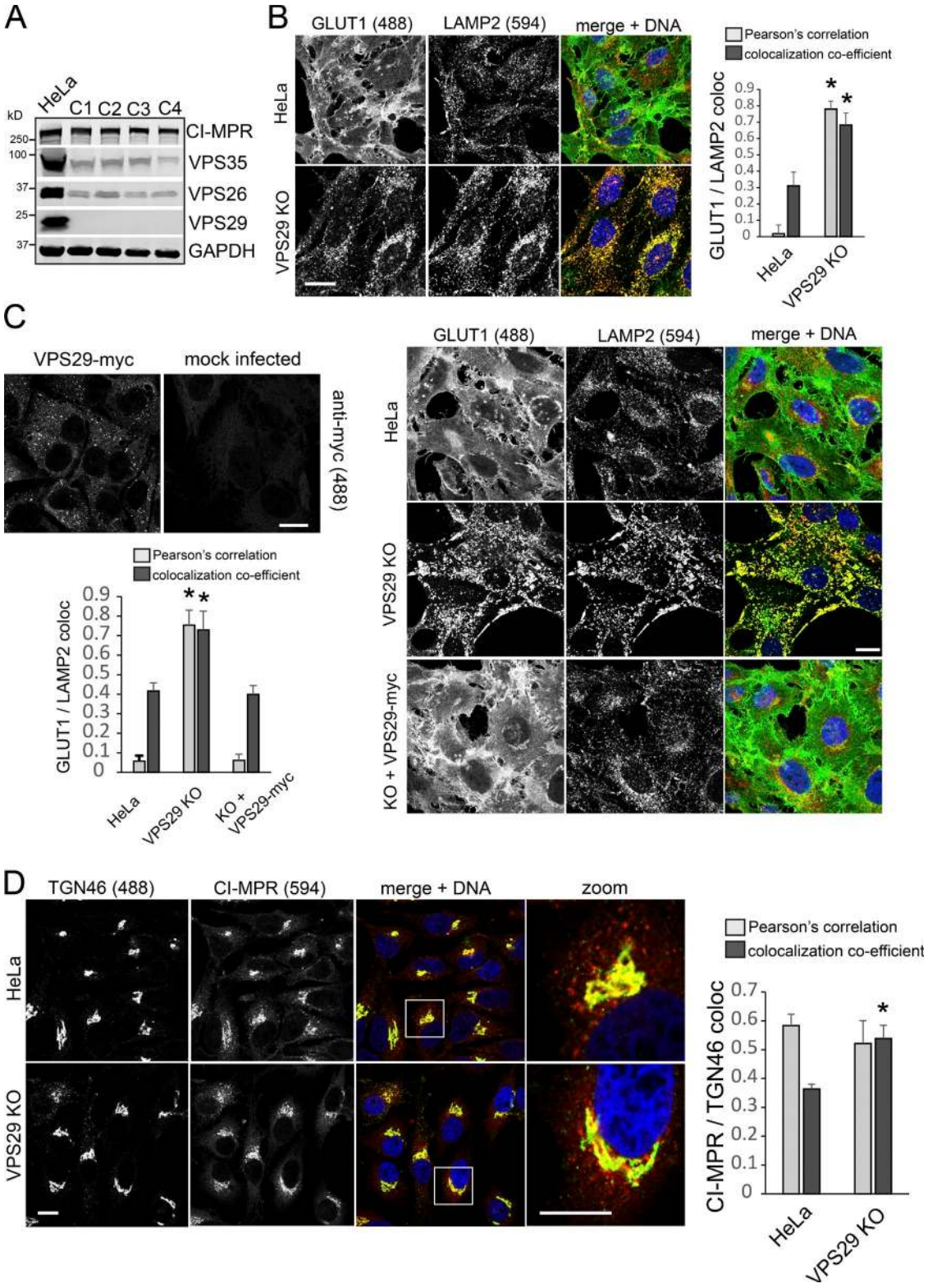

Figure 2. **KO of VPS29 does not result in loss of CI-MPR or CI-MPR dispersal from the TGN.** (A) Western blot analysis of indicated proteins in parental HeLa cells and four VPS29-deficient cell lines generated with CRISPR-Cas9. (B) Immunofluorescence of endogenous GLUT1 (green) and endogenous LAMP2 (red) in HeLa cells and a VPS29-KO cell line. The colocalization was quantified across 16 images taken from two independent experiments. (C) Lentiviral reexpression of VPS29-myc fully restores GLUT1 localization at the plasma membrane. The colocalization was quantified across 12 images acquired in two independent experiments (D) Immunofluorescent staining of endogenous CI-MPR (red) and the endogenous TGN marker TGN46 (green) in parental HeLa and VPS29-KO cell lines. The colocalization was quantified across 12 images acquired in two independent experiments. Bars, 10 µm. Error bars indicate SD. *, $P < 0.05$ compared with control conditions in a *t* test.

Downloaded from http://rupress.org/jcb/article-pdf/216/11/3677/1374505/jcb_201702137.pdf by guest on 26 August 2022

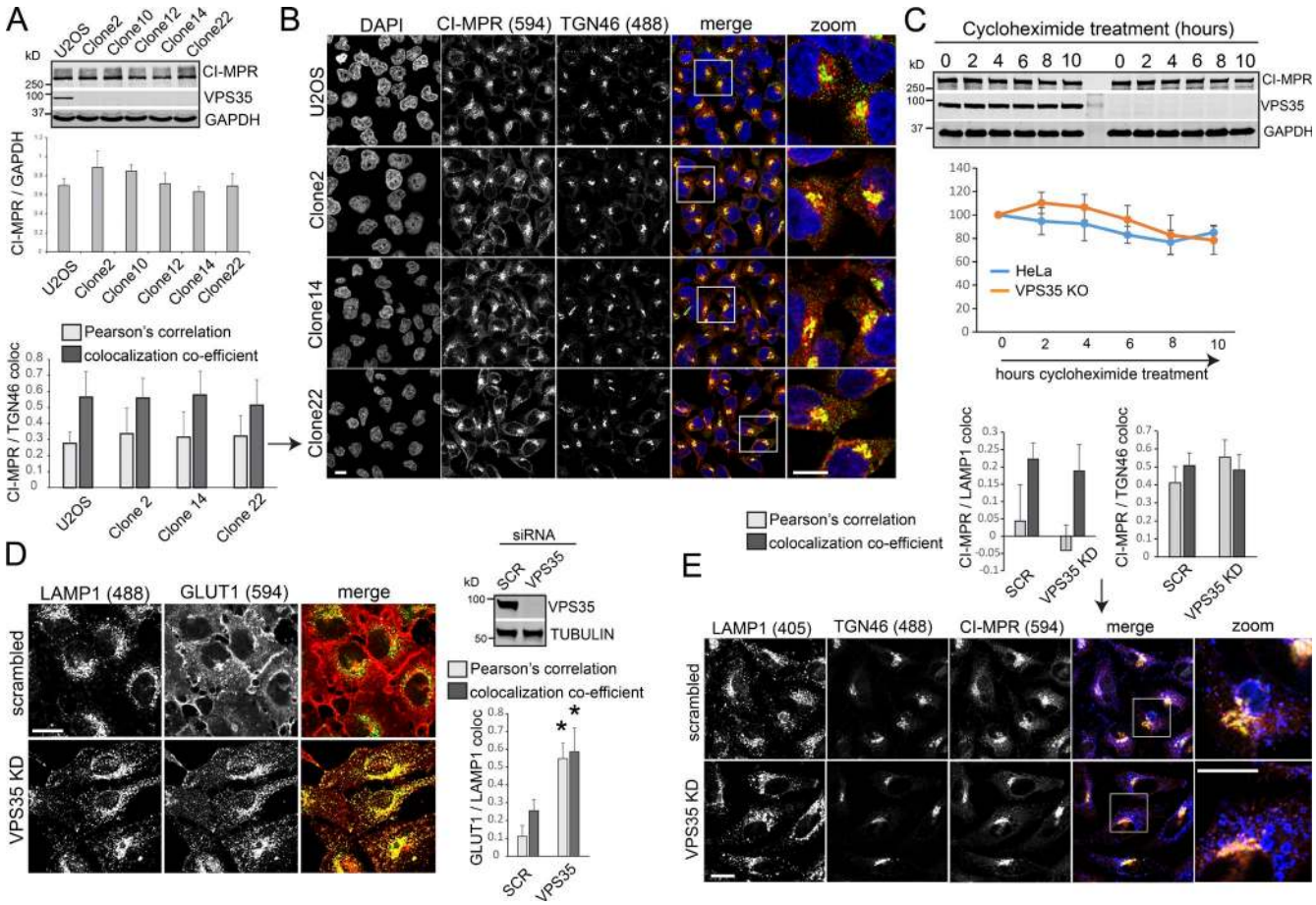

Figure 3. **TALEN-mediated deletion of VPS35 in U2OS and knockdown of VPS35 in HeLa cells does not cause retrograde sorting defects of CI-MPR.** (A) Western blot analysis of clonal U2OS osteosarcoma cells with a TALEN-mediated disruption of exon 4 of the VPS35 gene. The graph displays the level of endogenous CI-MPR/GAPDH quantified over three independent experiments. (B) Immunofluorescent staining of endogenous CI-MPR and endogenous TGN46 in human U2OS, with colocalization quantified over three independent experiments. (C) CI-MPR degradation experiment in U2OS cells treated with the ribosome inhibitor cycloheximide for the indicated periods. The abundance of CI-MPR was adjusted by the GAPDH signal and quantified over three independent experiments. (D) Immunofluorescent staining of endogenous GLUT1 (red) and endogenous LAMP1 (green) in HeLa cells treated with scrambled and VPS35-specific siRNA. The colocalization between LAMP1 and GLUT1 was quantified across 12 images acquired in two independent experiments. The knockdown (KD) efficiency was verified by Western blotting. (E) Immunofluorescent staining of endogenous CI-MPR (red) with the lysosomal marker LAMP1 (blue) and the TGN marker TGN46 (green). The colocalization of CI-MPR with the two markers was quantified over three independent experiments. Bars, 10 µm. Error bars indicate SD. *, $P < 0.05$ compared with control conditions in a *t* test.

MPR from the TGN46-stained TGN. Although targeting of the two GGAs led to an increase in TGN localization, only disruption of SNX1/2 or SNX5/6 led to a pronounced loss of TGN localization. Deletion of RAB7A and clathrin completely disrupted CI-MPR and also TGN46 localization, which is known to cycle from endosomes to the TGN (Roquemore and Banting, 1998), thereby further confirming efficiency of our CRISPR-Cas9 screen (Fig. 4 G). Neither disruption of the SNX-BARs nor deletion of VPS35 affected retrograde sorting of TGN46, which indicates that TGN46 utilizes alternative retrograde transport mechanisms that operate independently from retromer but also depend on RAB7a. It should also be noted here that the AP-1 complex has been implicated in the retrograde transport of CI-MPR (Meyer et al., 2000; Robinson et al., 2010), a phenotype that we failed to detect in this study. Although our Western blots indicated a pronounced loss of AP1B1 protein (~90%) after CRISPR treatment, we cannot entirely rule out that residual protein obscured these reported effects.

In the following experiments, we isolated clonal SNX1/2 and SNX5/6 double-KO cell lines and analyzed these cell lines for a CI-MPR retrograde trafficking defect. Both SNX1/2- and SNX5/6-KO cells but not VPS35-KO cells displayed a pronounced loss of CI-MPR from the TGN (Fig. 5 A). All analyzed clones displayed similar CI-MPR dispersal phenotypes (Fig. S3 C). The double KO of SNX1/2 confirmed the constitutive nature of the SNX-BAR heterodimers as the clonal cell lines also displayed an almost complete loss of SNX5 and SNX6 (Fig. S3 D). Similarly, SNX1 levels dropped significantly in the SNX5/6-KO cell lines (Fig. S3 C). Double depletion of SNX1/2 with siRNA replicated the same dispersal phenotype, whereas depletion of VPS35 did not have an effect on CI-MPR localization in the same experiment (Fig. S4 A). Dynamic antibody uptake and chase assays with an antibody against endogenous CI-MPR over 30 and 60 min revealed a complete failure of the antibody–CI-MPR complex to reach the TGN in both SNX1/2- and SNX5/6-depleted cells (Fig. 5 B). Importantly, lentiviral reexpression of either GFP-SNX5 or GFP-SNX6 rescued the loss of CI-MPR from the TGN (Fig. 5 C), indicating that the clonal KO cell lines did not have off-target defects that impacted upon CI-MPR sorting.

Downloaded from http://rupress.org/jcb/article-pdf/216/11/3677/1374505/jcb_201702137.pdf by guest on 26 August 2022

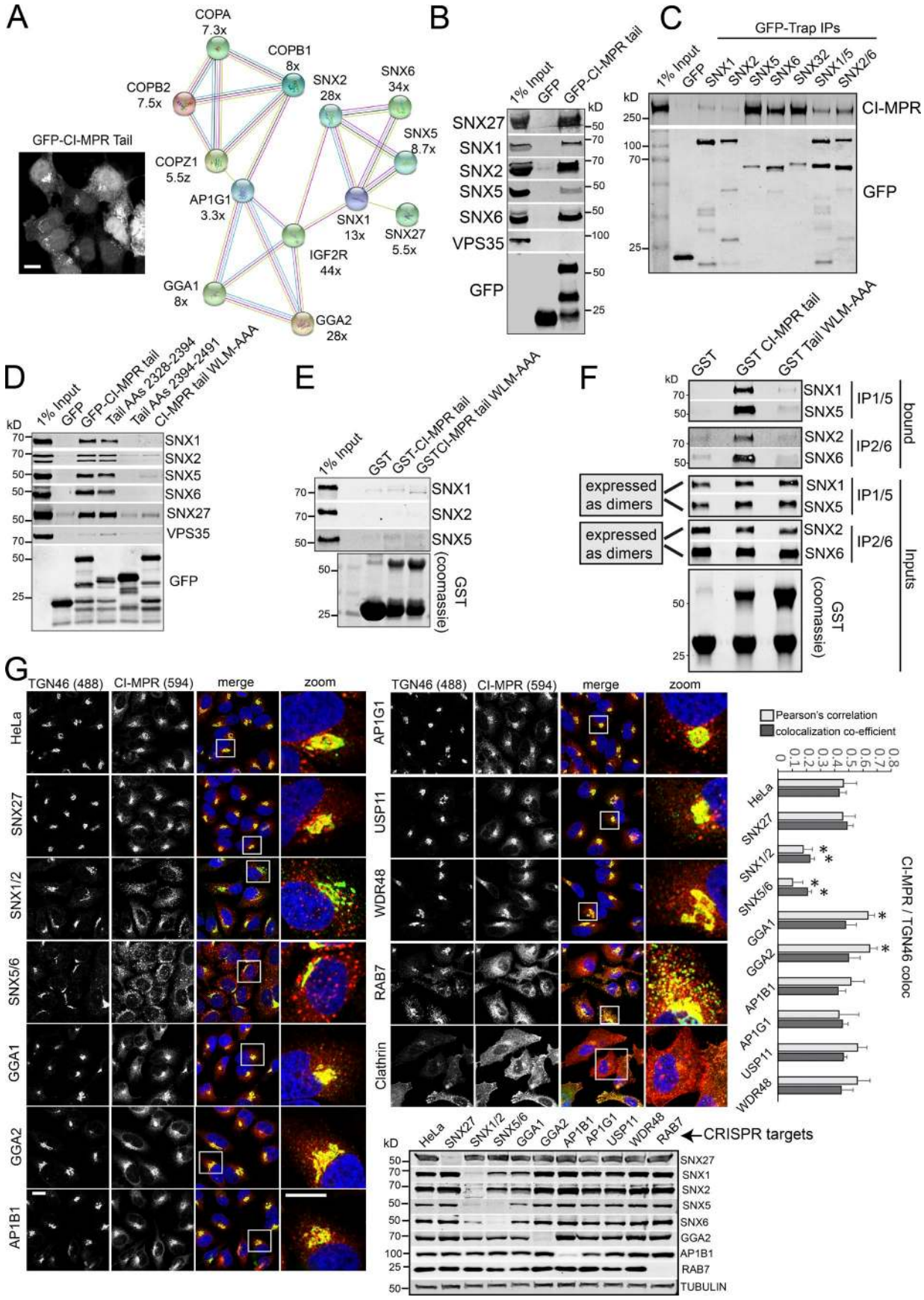

Downloaded from http://rupress.org/jcb/article-pdf/216/11/3677/1374505/jcb_201702137.pdf by guest on 26 August 2022

The SNX-BARs mediate export from sorting endosomes

If the SNX-BARs mediate export of the CI-MPR from retromer-positive sorting endosomes to the TGN, KO of the SNX-BARs should lead to an accumulation in a compartment positive for markers like the endosomal marker EEA1 and also for retromer. Indeed, costaining of endogenous EEA1 and CI-MPR in SNX1/2 and SNX5/6 double-KO cell lines revealed an almost complete redistribution of CI-MPR to an EEA1-positive compartment (Fig. 6 A). Costaining of CI-MPR and endogenous VPS35 in SNX1/2-KO, SNX5/6-KO (Fig. 6 B), and SNX1/2-depleted cells (Fig. S4 B) as well as dynamic CI-MPR antibody uptake assays in the KOs (Fig. S4 C) indicated that the endosomes that CI-MPR aberrantly accumulated in were VPS35 positive. We also detected the late endocytic marker RAB7 on those endosomes, suggesting that they are larger sorting endosomes with EEA1-, VPS35-, and RAB7-decorated subdomains (Fig. S4 D). In spite of a clear shift in localization to a VPS35-decorated endosome, colocalization parameters increased only modestly as VPS35 and CI-MPR signals were juxtaposed on the same endosome (Figs. 6 B and S4, B and C). The same juxtapositioning was observed in WT HeLa cells, where high-magnification confocal and stimulated emission depletion (STED) superresolution imaging showed that vesicular CI-MPR and VPS35 resided in distinct subdomains of the same complex-sorting endosome (Fig. 6 C). In contrast, endogenous SNX1 fully colocalized with CI-MPR on the limiting membrane of these endosomes (Fig. 6 C). In agreement with this, we found that endogenous SNX1 and VPS35 overlapped in some regions of the endosome but also formed separated subdomains (Fig. 6 C). We failed to detect enhanced degradation rates of CI-MPR in cells treated with siRNA against SNX1/2 (Fig. S4 E). SNX1/2 and SNX5/6 double KO cell lines displayed slightly enhanced CI-MPR degradation kinetics compared with parental HeLa cells (Fig. S4 F).

Finally, we investigated whether targeting of the SNX-BAR binding site within the CI-MPR protein replicated the loss of retrograde transport to the TGN. Using a CRISPR-Cas9 construct cutting within the WLM motif that the SNX-BARs bind to, we isolated a clonal cell line with an in-frame deletion of 18 nucleotides, resulting in a deletion of six amino acids that included the WLM motif of the endogenous CI-MPR locus (Fig. S4 G). This mutant CI-MPR lost its TGN localization and distributed to an endosomal compartment, similar to the effect of SNX-BAR deletion (Fig. 7, A and B). We also reexpressed full-length WT CI-MPR and the WLM-AAA mutant in CI-MPR–KO HeLa cells, which also revealed a dispersal of the SNX-BAR–binding mutant receptor from the TGN (Fig. 7 C). We concluded that CI-MPR is sorted to the TGN via SNX-BAR proteins from endosomal subdomains that may be spatially separated from domains decorated with the core retromer trimer. In the absence of the SNX-BARs, CI-MPR aberrantly accumulates in an EEA1-enriched subdomain of RAB7- and VPS35-positive sorting endosomes with a minor increase in lysosomal degradation.

The insulinlike growth factor receptor 1 (IGF1R) is also recycled through the SNX-BARs independently of retromer

To identify additional SNX-BAR–dependent cargoes, we performed SILAC-based quantitative interactome analysis all four GFP-tagged SNX-BAR proteins. The proteomics strikingly revealed the heterodimeric and also oligomeric nature of the SNXs, as the top hits for each SNX were all three other SNX-BAR proteins (Fig. 8 A and Table S2). Our interactome screen identified the previously reported interactors SNX27 (Steinberg et al., 2013) and RME-8 for SNX1 (Popoff et al., 2009) and VAPA/VAPB for SNX2 (Dong et al., 2016), confirmed the binding of SNX5 and SNX6 to CI-MPR, and also identified transmembrane proteins such as MRP1, basigin, or semaphorin-4C as potential additional cargoes. Intriguingly, SNX5 appeared to robustly precipitate the IGF1R as well as traces of the insulin receptor (INSR), which may be because of heterodimeric IGF1R/INSR hybrid receptors (Fig. 8 A and Table S2; García-de Lacoba et al., 1999). Indeed, Western blotting of the SNX-BAR GFP-trap isolates confirmed binding of SNX5 to the IGF1R, whereas we could not detect INSR (Fig. 8 B), suggesting that the more sensitive mass spectrometer–detected traces of INSR coprecipitated with the IGF1R. The isolated GFP-tagged tail of the IGF1R and semaphorin-4C but not that of the INSR efficiently precipitated endogenous SNX5 and weakly precipitated endogenous SNX6 (Fig. 8 C). Recombinant GST-tagged tails of the IGF1R, semaphorin-4C, and CI-MPR bound efficiently to recombinant SNX1/5 and SNX2/6 dimers, indicating direct interactions. Functionally, we found that endogenous IGF1R is internalized into an SNX1-decorated compartment in MCF-7 cells treated with IGF-1 (Fig. 8 E). Degradation assays without IGF-1 stimulation in cycloheximide-treated SNX1/2 and SNX5/6 KO HeLa cells revealed a slightly decreased stability of the endogenous IGF1R in all clones tested, whereas the INSR was unaffected (Figs. 8 F and S5 A). In contrast, IGF1R stability was unaffected in two VPS35-KO clonal cell lines (Fig. S5 B) Next, we tested whether activation of the IGF1R through its ligand IGF-1 would increase its dependence on SNX-BAR–mediated recycling. Indeed, when the cells were starved of serum overnight and then treated with 10 nM IGF-1, stability of the

Figure 4. **SNX-BAR dimers directly bind to the CI-MPR tail to promote retrograde sorting to the TGN.** (A) The GFP-tagged CI-MPR tail and GFP only were lentivirally expressed in SILAC-labeled HEK293 cells and precipitated with GFP-trap beads, and then interacting proteins were identified by LC-MS/MS. The panel shows a STRING network analysis of CI-MPR tail–interacting proteins. The numbers beneath each protein indicate the fold enrichment of the protein when compared with the GFP-only control. (B) Western blot–based verification of the interacting proteins. (C) GFP-trap IPs of the indicated GFP-tagged SNX-BAR proteins precipitating the endogenous CI-MPR from HEK293 cells. (D) GFP-trap IPs of the GFP-tagged WT CI-MPR tail and of the indicated mutant CI-MPR tail constructs were probed for the presence of the indicated endogenous SNXs and endogenous VPS35 by Western blotting. (E) Direct recombinant interaction assay with GST-tagged CI-MPR tail produced in bacteria and the indicated individual His-tagged SNX-BAR proteins produced as secreted proteins in HEK293 cells. (F) Direct recombinant interaction assay with GST-tagged CI-MPR tail produced in bacteria, and the indicated His-tagged SNX-BAR proteins coexpressed as secreted proteins in HEK293 cells. (G) Three CRISPR constructs per indicated gene targeting distinct genomic regions of the respective gene were pooled and cotransfected with a puromycin resistance–encoding plasmid. After puromycin selection and recovery for 3 d, cells were seeded onto coverslips, and CI-MPR localization to the TGN was analyzed by immunofluorescent staining of endogenous CI-MPR (red) and endogenous TGN46 (green). The screen was performed twice, and the colocalization (coloc) between CI-MPR and TGN46 was quantified over 20 images per condition acquired in the two experiments. The efficiency of the respective CRISPR-Cas9 treatment was verified by Western blotting against selected targets. Bars, 10 µm. Error bars indicate SD. *, $P < 0.05$ compared with control conditions in a *t* test.

Downloaded from http://rupress.org/jcb/article-pdf/216/11/3677/1374505/jcb_201702137.pdf by guest on 26 August 2022

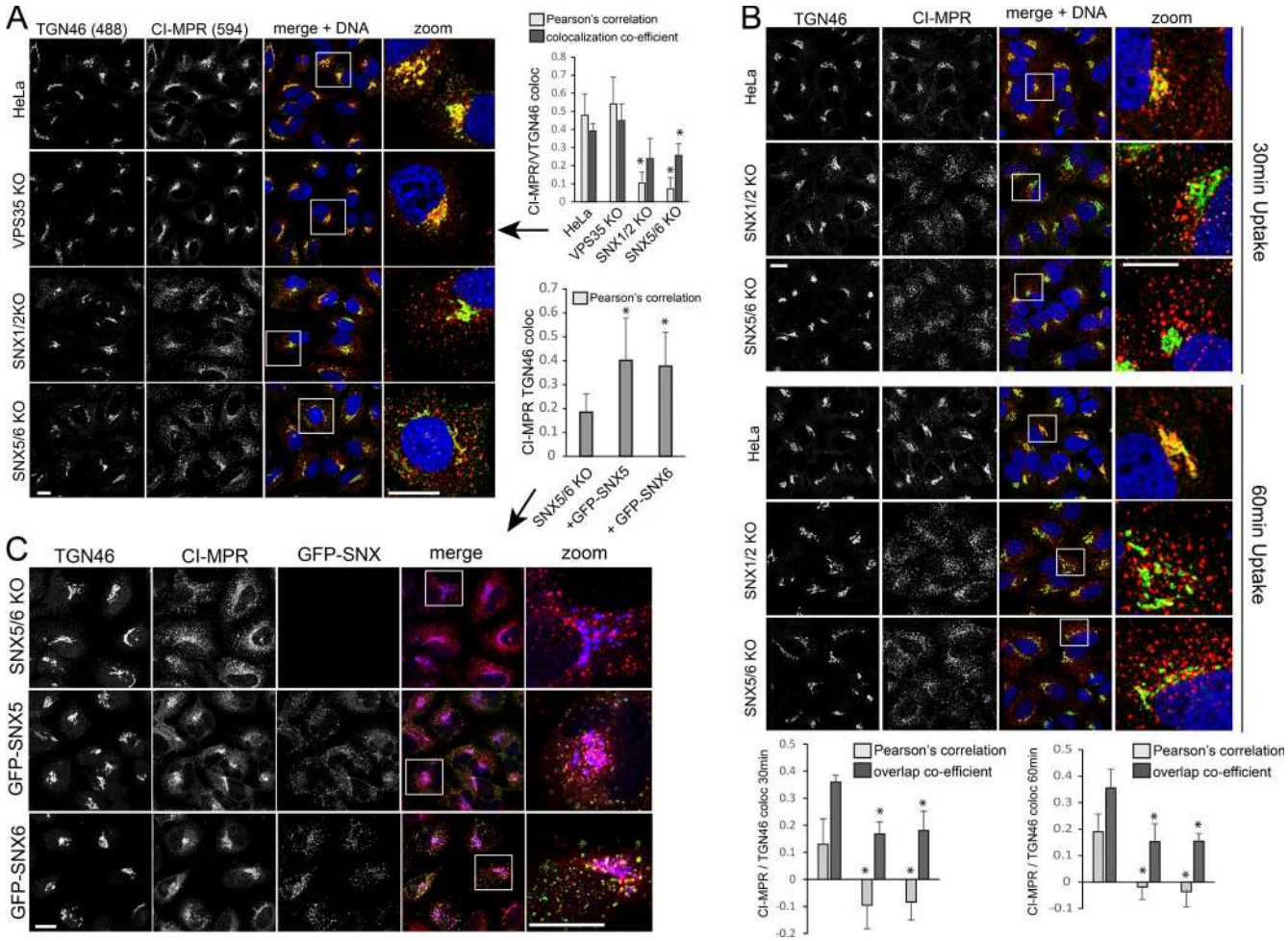

Figure 5. **KO of the SNX-BAR proteins causes a complete loss of retrograde sorting of the CI-MPR in HeLa cells.** (A) Immunofluorescent analysis of the endogenous CI-MPR (red) and endogenous TGN46 (green) in clonal VPS35 and SNX1/2 and SNX5/6 double-KO cells. The colocalization was quantified over three independent experiments. (B) Uptake assay with an antibody against the extracellular domain of the endogenous CI-MPR over 30 and 60 min of uptake at 37°C. Delivery of the antibody/receptor duplex to the TGN was analyzed through costaining of the internalized antibody (red) with endogenous TGN46 (green). The colocalization was quantified over three independent experiments. (C) GFP-tagged SNX5 and GFP-tagged SNX6 were lentivirally expressed in SNX5/6 double-KO cells lines, and localization of endogenous CI-MPR (red) and endogenous TGN46 (blue) was quantified over three independent experiments. Bars, 10 µm. Error bars indicate SD. *, $P < 0.05$ compared with control conditions in a *t* test.

IGF1R was dramatically decreased in SNX1/2 and SNX5/6 but not in VPS35 KO cells over long (Fig. 9 A) and short (Fig. S5 C) IGF-1 stimulation periods. A microscopic analysis of lentivirally expressed IGF1R-myc in HeLa cells revealed no apparent changes to IGF1R localization under serum-starved conditions in SNX-BAR and VPS35 KO cells compared with control HeLa cells (Fig. 9 B). After 1 h IGF-1 stimulation, the IGF1R strongly accumulated in intracellular vesicles, which were partially costained for the lysosomal marker LAMP1 in SNX-BAR–KO cells, whereas it remained mainly at the plasma membrane in control and VPS35-KO cells (Fig. 9 B). Costaining of the IGF1R with endogenous RAB7 or VPS35 in IGF-1–stimulated SNX1/2- and SNX5/6-KO cells showed that the accumulated IGF1R often resided in the same endosomal structure as VPS35 or RAB7 but in a distinct subdomain (Fig. S5 D). The effects of SNX-BAR deletion were specific for the IGF1R, as we could not detect any changes in INSR turnover in insulin-stimulated cells (Fig. 9 C). Furthermore, the enhanced degradation of the IGF1R could be fully reverted by lentiviral reexpression of either GFP-SNX5 or GFP-SNX6 (Fig. 9 D). Notably, expression of GFP-SNX5 or GFP-SNX6 also increased overall IGF1R levels in the KO cells (Fig. 9 D). In agreement with enhanced lysosomal degradation, treatment of the IGF-1–stimulated SNX5/6 KO cells with the lysosomal inhibitor bafilomycin-A1 abolished the increased degradation rates (Fig. 9 E). We concluded that SNX-BAR proteins, but not the retromer trimer, are required for the recycling of the ligand-activated IGF1R from sorting endosomes, which prevents entry into the lysosomal pathway.

Discussion

In this study, we have demonstrated that endosomal recycling and retrograde transport of the CI-MPR as well as recycling of the IGF1R depends on direct engagement of heterodimeric combinations of SNX1 and SNX2 with SNX5 and SNX6 without any measurable role for the core retromer trimer composed of VPS26, VPS29, and VPS35. We admittedly have difficulties explaining the apparent differences between our results and previously published data (Arighi et al., 2004; Seaman, 2004, 2007). Some of the older research relied on suppression of VPS26A (Arighi et al., 2004), an approach that may not

Downloaded from http://rupress.org/jcb/article-pdf/216/11/3677/1374505/jcb_201702137.pdf by guest on 26 August 2022

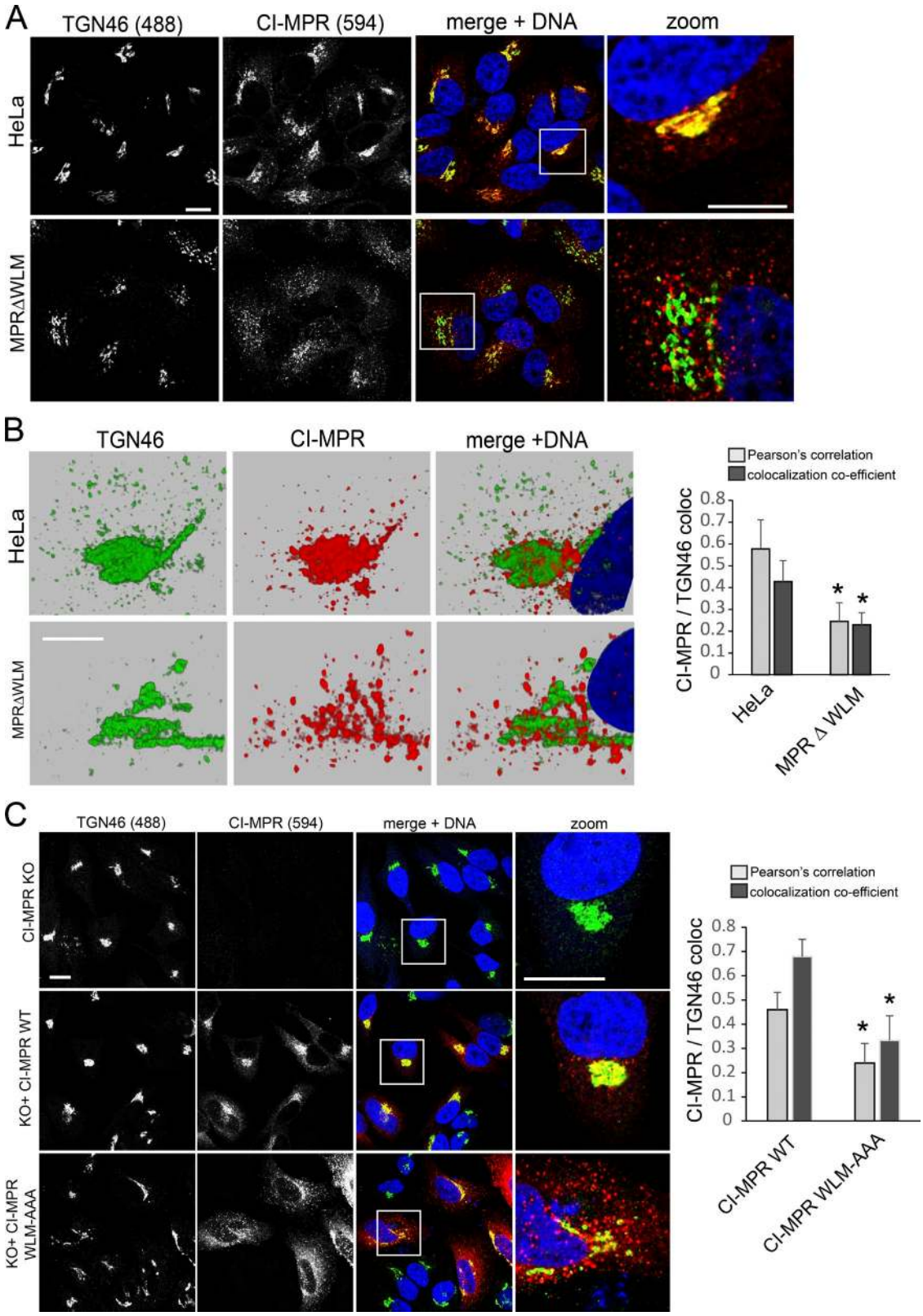

Figure 6. **Genomic deletion of the SNX-BAR binding site abrogates retrograde transport of endogenous as well as reexpressed CI-MPR.** (A) CRISPR-Cas9 was used to introduce a 6-aa deletion of the WLM SNX-BAR binding motif into the endogenous CI-MPR locus of a HeLa cell line. The immunofluorescence shows the colocalization between endogenous CI-MPR and the TGN marker TGN46. (B) 3D reconstruction of the CI-MPR and TGN46 staining in a HeLa cell and in a cell carrying the SNX-BAR–binding site deletion. The colocalization between CI-MPR and TGN46 was quantified over three independent experiments. (C) Reexpression of WT and WLM-AAA CI-MPR in a CI-MPR–KO HeLa cell line. The transfected cells were stained for CI-MPR and endogenous TGN46, and colocalization was quantified over three independent experiments. Bars, 10 µm. Error bars indicate SD. *, $P < 0.05$ compared with control conditions in a *t* test.

Downloaded from http://rupress.org/jcb/article-pdf/216/11/3677/1374505/jcb_201702137.pdf by guest on 26 August 2022

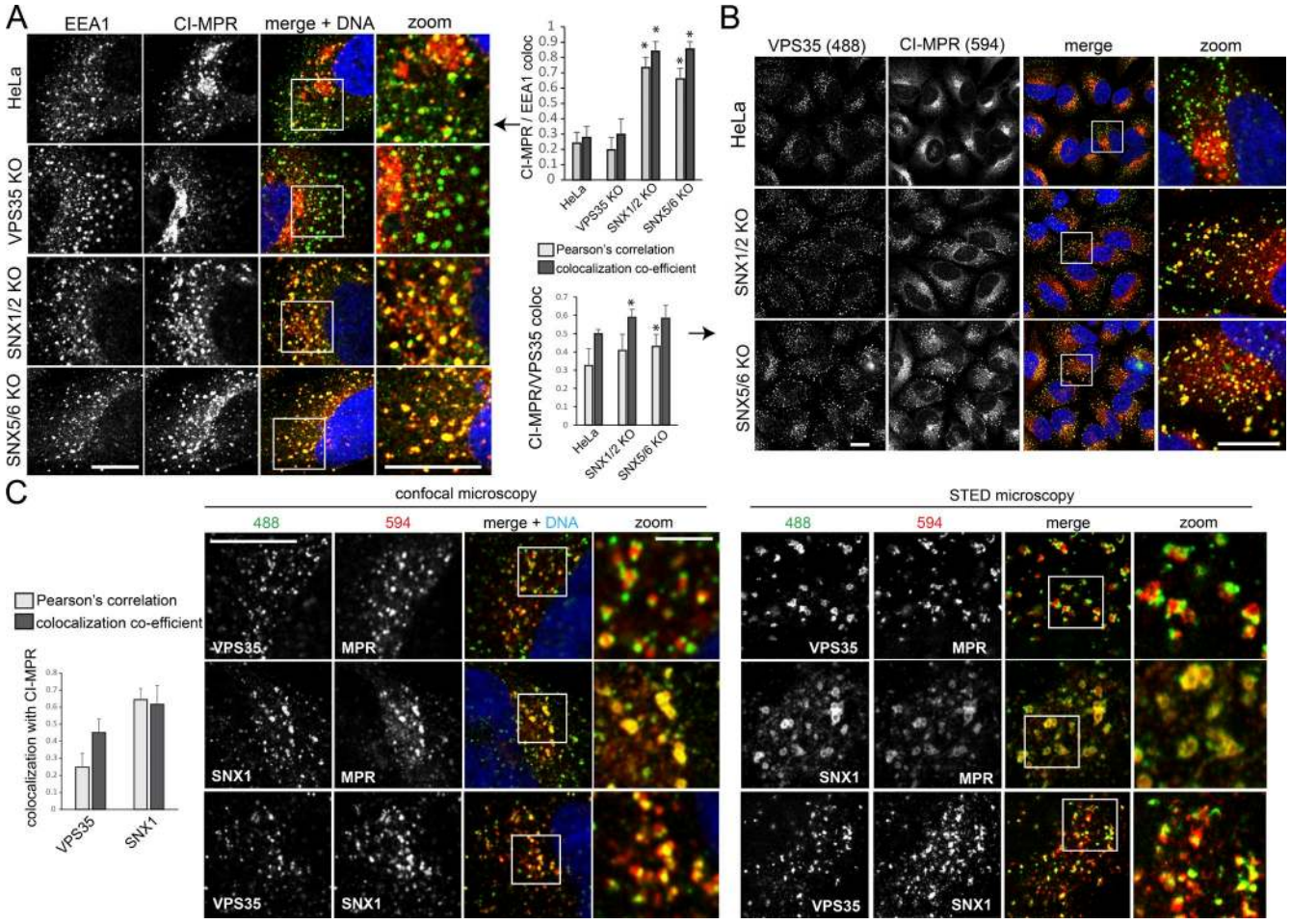

Figure 7. **The CI-MPR accumulates in VPS35-positive sorting endosomes but does not localize to the VPS35-decorated subdomain.** (A) Immunofluorescent staining of endogenous CI-MPR (red) and endogenous EEA1 (green) in HeLa cells and clonal VPS35, SNX1/2, and SNX5/6 double-KO cell lines. The colocalization was quantified over three independent experiments. (B) Immunofluorescent staining of endogenous CI-MPR (red) and endogenous VPS35 (green) in HeLa cells and clonal SNX1/2 and SNX5/6 double-KO cell lines. The colocalization was quantified over three independent experiments. (C) Costaining of indicated endogenous proteins in WT HeLa cells and analysis of colocalization by conventional confocal microscopy and STED superresolution microscopy. The colocalization between CI-MPR and VPS35 and CI-MPR and SNX1 was quantified across 12 images acquired in two independent experiments with conventional confocal microscopy. Bars: (main images) 10 µm; (insets) 3 µm. Error bars indicate SD. *, $P < 0.05$ compared with control conditions in a *t* test.

have been optimal in light of the relatively recent discovery of VPS26B (Collins et al., 2008), which we found to be the functional equivalent of VPS26A (Gallon et al., 2014). In our hands, only simultaneous targeting of VPS26A and VPS26B resulted in a loss of retromer function, so that depletion of only one of the VPS26 isoforms may cause changes in retromer functionality that we do not yet understand (Gallon et al., 2014). We would also like to stress that the subcellular distribution of CI-MPR is far from uniform across cells, so that the frequently used visual scoring assays for dispersal of CI-MPR (Hao et al., 2013) may not have been robust enough to identify the lack of an effect of VPS trimer suppression. On a more fundamental level, our data indicate that the current working model of the retromer complex may have to be revised, as the VPS trimer and the four "retromer" SNX-BAR proteins seem to operate independently of one another. Sorting of the WNT growth factor transporting receptor Wntless through the SNX3–retromer complex was shown to be independent from the SNX-BARs (Harterink et al., 2011), whereas depletion of the SNX-BARs does not phenocopy the GLUT1 sorting defects seen upon suppression of the SNX27–retromer complex (Steinberg et al., 2013). However, the SNX-BARs and the core retromer do function together in the recycling of CED-1 for apoptotic cell clearance, a phenotype that was observed in *Caenorhabditis elegans* (Chen et al., 2010). To our knowledge, biochemical evidence for an interaction of the VPS trimer and the SNX-BARs in mammalian cells is scarce, and the functional connection between retromer and the SNX-BAR proteins was mainly based on their communal role in the sorting of CI-MPR, which we could not confirm in this study. The heteropentameric (or rather, septameric in mammals) nature of retromer was discovered in yeast, where the VPS26–VPS29–VPS35 trimer forms a stable and functional complex with the SNX1/2 and SNX5/6 equivalents VPS5p and VPS17p (Seaman et al., 1998). It appears conceivable that the core retromer trimer and the SNX-BAR proteins have functionally diverged during evolution alongside the apparent loss of their physical interactions. Our data indicate that the SNX-BARs and the VPS trimer do not fully colocalize and may even form somewhat separated subdomains on the same endosome, with CI-MPR only enriched in the SNX-BAR–decorated part. The SNX-BAR proteins have intrinsic PI3P affinity through their Phox homology (PX) domain (Haft et al., 1998; Zhong et

Downloaded from http://rupress.org/jcb/article-pdf/216/11/3677/1374505/jcb_201702137.pdf by guest on 26 August 2022

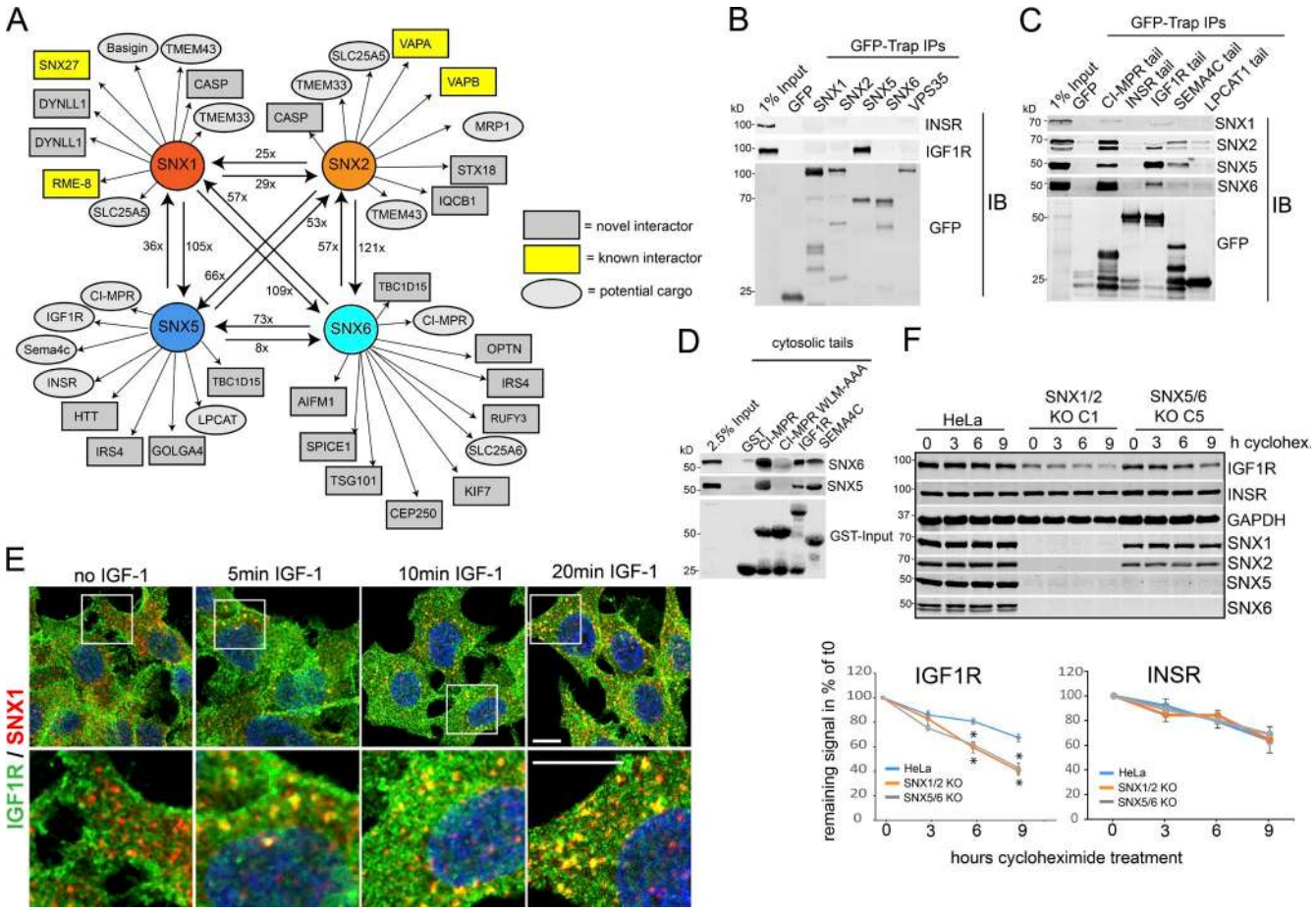

Figure 8. **Proteomic quantification of the SNX-BAR interactome identifies the IGF1R as a SNX-BAR interactor.** (A) GFP-tagged SNX1, SNX2, SNX5, and SNX6 were transiently expressed in SILAC-labeled HEK293 cells. GFP-only was expressed in nonlabeled HEK293 cells as a control. The SNX-BARs and GFP were precipitated with GFP-trap beads, each SNX-BAR IP was pooled with a GFP-only IP, and the combined samples were quantified by LC-MS/MS. The panel displays the fold enrichment of the other SNX-BARs in each individual SNX-BAR precipitation, indicating robust heterodimerization and multimerization between the SNX-BARs. Selected other interactors of the respective SNX-BAR protein at least fivefold enriched over the GFP-only control are indicated by arrows. (B) GFP-trap IPs of the indicated SNX-BARs and analysis of the presence of the endogenous IGF1R and the INSR in the precipitates. (C) GFP-trap IPs of the isolated cytoplasmic tails of selected potential SNX-BAR cargoes and analysis of the presence of the endogenous SNX-BAR protein in the precipitates. IB, immunoblot. (D) Direct recombinant interaction with the GST-tagged cytosolic tails produced in bacteria and His-tagged SNX5, and SNX6 coexpressed with His-tagged SNX1 and SNX2, respectively. (E) Immunofluorescent staining of endogenous IGF1R (green) and endogenous SNX1 (red) in serum-starved MCF-7 cells treated with 10 nM IGF-1 for the indicated periods. (F) Degradation assay of endogenous IGF1R and the INSR in HeLa cells, and clonal SNX1/2 and SNX5/6 double-KO cells lines treated with the ribosomal inhibitor cycloheximide for the indicated periods. The degradation kinetics were quantified over four independent experiments. Bars, 10 µm. Error bars indicate SD. *, $P < 0.05$ compared with control conditions in a *t* test.

al., 2002), detect or induce local curvature (Carlton et al., 2004), tubulate membrane (van Weering et al., 2012), and directly bind cargo, thereby fulfilling most requirements for carrier formation without the need for the VPS trimer. Several SNX-BAR–interacting accessory proteins have also been reported with additional roles in carrier formation. Although binding of SNX1 to RME-8 probably removes endosomal clathrin during cargo enrichment and may also alter actin dynamics to promote tubule scission (Shi et al., 2009; Freeman et al., 2014), SNX2 engages VAPA/VAPB to establish endosome–ER contact sites, which are important for efficient recycling and phosphoinositide dynamics (Dong et al., 2016). Our proteomics suggest that SNX5 and SNX6 also interact with the RAB7 GAP TBC1D15 (Zhang et al., 2005; Peralta et al., 2010), which may be needed to turn off RAB7 activity before/during carrier formation and also with several golgins—most notably GolginA4, which has recently been shown to be a functional tether for mannose phosphate receptor–bearing carriers (Wong and Munro, 2014). Overall, it appears that the retromer SNX-BARs possess all the requirements to form functional carriers from sorting endosomes in the absence of core retromer function.

Although our data strongly suggest that SNX5 and SNX6 are the cargo-selective elements within the SNX-BAR dimers, it remains to be conclusively shown how this binding is achieved and whether dimerization is really needed for cargo engagement. In this context, it was somewhat puzzling that GFP-SNX1 and GFP-SNX2, which efficiently dimerize with SNX5 and SNX6 (Wassmer et al., 2007, 2009), precipitated hardly any CI-MPR. One possibility is that the GFP tag of SNX1 or SNX2 sterically interferes with the CI-MPR binding site in SNX5 and SNX6. It is also conceivable that the reported homodimerization of SNX1 and SNX2 (Carlton et al., 2004; van Weering et al., 2012) occurs very efficiently when these proteins are overexpressed, which would exclude SNX5 and SNX6 from the SNX1- and SNX2-generated endosomal tubules. This in turn would result in inefficient CI-MPR engagement through heterodimerization

Downloaded from http://rupress.org/jcb/article-pdf/216/11/3677/1374505/jcb_201702137.pdf by guest on 26 August 2022

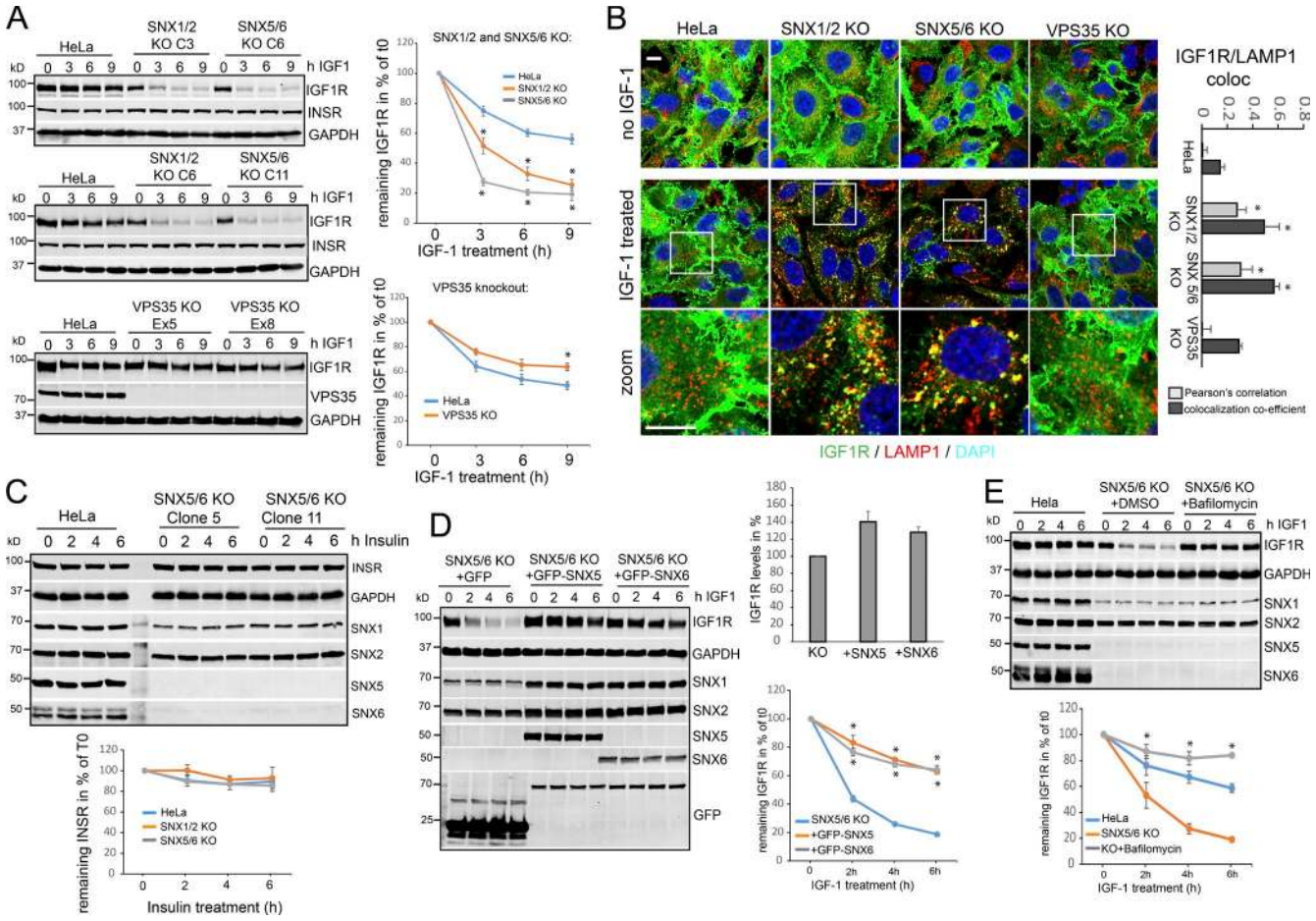

Figure 9. **The SNX-BAR proteins are needed to prevent lysosomal degradation of the activated IGF1R.** (A) HeLa cells, clonal SNX1/2 and SNX5/6 double-KO cells, and two VPS35-KO cell lines were serum starved and treated with 10 nM IGF-1 for the indicated periods. The level of endogenous IGF1R and the INSR were detected by Western blotting, and the IGF1R degradation kinetics were quantified over four independent experiments. (B) HeLa cells, clonal SNX1/2, and SNX5/6 double-KO cells as well as VPS35-KO cell lines were transduced with a lentiviruses expressing human IGF1R-myc, serum starved, and then treated with 10 nM IGF-1 for 1 h. The IGF1R and endogenous LAMP1 were stained by immunofluorescence, and the colocalization was quantified across 16 images acquired in two independent experiments. (C) HeLa cells and SNX1/2 and SNX5/6 double-KO cell lines were serum starved and treated with 5 µg/ml insulin for the indicated periods, and the level of the endogenous INSR was quantified by Western blotting over three independent experiments. (D) SNX5/6 double-KO cells were transduced with lentiviruses expressing GFP-SNX5 or GFP-SNX6 and with GFP only as a control. The cells were serum starved and treated with 10 nM IGF-1 for the indicated periods, followed by Western blot–based detection of the levels of the endogenous IGF1R. The level of the endogenous IGF1R in starved cells (top bar graph) as well as the degradation kinetics in IGF-1–treated cells were quantified over four independent experiments. (E) HeLa cells and clonal SNX5/6 double-KO cells were serum starved and treated with 10 nM IGF-1 for the indicated periods. One set of the SNX5/6 KO cells was treated with the lysosomal inhibitor bafilomycin-A1. The degradation kinetics were quantified over four independent experiments. Bars, 10 µm. Error bars indicate SD. *, $P < 0.05$ compared with control conditions in a *t* test.

with SNX5 and SNX6. While this manuscript was under preparation, it was reported the *Chlamydia trachomatis* protein Inc.E binds to a hydrophobic grove around F136 in the PX domain of SNX5, which was also shown to displace CI-MPR from SNX5 (Elwell et al., 2017). Comparative proteomics of mutant (SNX5 F136D and SNX5Y132D) and WT SNX5 revealed a loss of CI-MPR and also of IGF1R binding, which confirms our binding data on CI-MPR and IGF1R and suggests a common binding site within the PX domain of SNX5.

The apparent binding to the IGF1R and our discovery that recycling of the IGF1R also depends on the SNX-BAR proteins are other interesting aspects of our study. It is far from obvious why both mammalian IGF receptors, which are evolutionary and structurally unrelated, rely on the same endosomal sorting mechanism. The CI-MPR regulates extracellular levels of IGF-2 and thereby IGF1R and likely INSR activity in embryonic development (Ludwig et al., 1996; Dupont and Holzenberger, 2003), making a shared and potentially regulated recycling loop conceivable. On an experimental level, the robust and easily quantifiable degradative phenotype of endogenous IGF1R upon loss of the SNX-BARs will be of tremendous value to further dissect the mechanics of SNX-BAR carrier formation. It is also not clear how the SNX-BARs achieve endosome-to-TGN and endosome-to-plasma membrane recycling. A likely explanation is that the SNX-BARs merely mediate the exit from an early endosomal/sorting endosomal and degradation-competent compartment as well as subsequent transport into a communal recycling compartment, which is continuous with a TGN/post-Golgi secretory compartment, from which further sorting decisions are taken. Evidence for this has been reported in the early days of research into CI-MPR trafficking (Lin et al., 2004) and also recently for the retromer cargoes Wntless and the β2-adrenergic receptor, which also take divergent trafficking routes after being sorted by retromer (Varandas et al., 2016). Overall, our data do

Downloaded from http://rupress.org/jcb/article-pdf/216/11/3677/1374505/jcb_201702137.pdf by guest on 26 August 2022

not support the current working model of the retromer complex and call the functional composition of retromer as a complex of the VPS trimer and the SNX-BAR proteins into question.

Materials and methods

Antibodies

Antibodies used in this study were: From Abcam: rabbit anti–CI-MPR (ab124767), rabbit anti-LAMP1 (ab24170), rabbit anti-GLUT1 (ab15309), rabbit anti-VPS35 (ab97545), rabbit anti-VPS26 (ab181352), rabbit anti-VPS29 (ab98929), mouse anti-SNX27 (ab77799), rabbit anti-SNX5 (ab18520), and rabbit anti-INSR (ab131238). From BD: mouse anti-EEA1 (610457), mouse anti-SNX1 (611482), and mouse anti-SNX2 (611308). From AbD Serotec/Bio-Rad Laboratories: sheep anti-TGN46 (AHP500) and mouse anti–CI-MPR (anti-CD222; clone MEM-238). Further antibodies used were: rabbit anti–IGF1R β (9750; Cell Signaling Technology), mouse anti-GAPDH (10494-1-AP; Proteintech), rabbit anti-GGA2 (10356-1-AP; Proteintech), rabbit anti-AP1B1 (16932-1-AP; Proteintech), mouse anti-SNX6 (S6324; Sigma-Aldrich), rat anti-myc (clone 9E1; ChromoTek), and rat anti-GFP (clone 3H9; ChromoTek).

Quantitative Western blotting

All the Western blots in this study were acquired with an Odyssey SA system (LI-COR Biosciences) to detect fluorescently labeled secondary antibodies (all secondary antibodies were from LI-COR Biosciences). The respective band intensities were measured using the automatic background subtraction (mean top and bottom setting) of the Odyssey software. All quantifications were done across at least three independent experiments.

cDNA constructs

The SNX-BAR cDNA as well as the IGF1R and IGF2R cDNA was cloned from HeLa cell cDNA prepared with the Superscript-III kit (Invitrogen) using KAPA HiFi DNA polymerase (Kapa Biosystems). All site-directed mutagenesis was performed using the QuikChange method (Promega) of fully overlapping primers combined with the KAPA HiFi polymerase.

TALEN-mediated disruption of the VPS35 gene

Human U2OS osteosarcoma cells were transfected with two plasmids encoding paired TALEN arms targeting exon 4 of the human VPS35 gene using Lipofectamine 2000 (Invitrogen). The TALEN targeting sequence is detailed in Fig. S1 E. 5 d after transfection, 100 cells in 20 ml of DMEM were seeded into a 96-well plate (200 µl/well), and single clones were picked when large colonies had formed. The clonal cell lines were analyzed for VPS35 KO by Western blotting. Three VPS35-negative clonal cell lines were further analyzed by genomic sequencing to verify a full KO. For that, 600 bases with the TALEN cleavage site in the middle were amplified from genomic DNA and subcloned into pEGFP-C1 for sequencing. The detected frame-shifting mutations disrupting the VPS35 protein are detailed in Fig. S1 E.

CRISPR-Cas9

To genomically delete protein expression, the px330 plasmid was modified with gene-specific guide RNA (gRNA) targeting sequences according to the Zhang laboratory protocol (Cong et al., 2013). The gRNA- and CAS9-encoding px330 plasmids were cotransfected with a plasmid encoding GFP-tagged puromycin resistance using FuGENE HD (Promega). 24 h after transfection, cells were selected with 3 µg/ml puromycin for 24 h, followed by incubation for 3 d. 5 d after transfection, 100 cells in 20 ml of DMEM or Iscove's modified Dulbecco's medium were seeded into a 96-well plate (200 µl/well), and single clones were picked when large colonies had formed. The clonal cells were screened for loss of the VPS35 protein by Western blotting. All targeting sequences were designed with the single gRNA designer of the Broad Institute (http://portals.broadinstitute.org/gpp/public/analysis-tools/sgrna-design). To disrupt VPS35 at exon 5 and exon 8, px330 plasmids targeting exon 5 and exon 8 were designed with the following gRNA sequences: 5′-GTGGTGTGCAACATCCCTTG-3′ (exon 5) and 5′-GAAAAGGATTCAAAGTCTGG-3′ (exon 8). All displayed individual clones starting with E5 (E5C1, E5C3, E5C7, and E5C19) were generated with the gRNA against exon 5, and all clones starting with E8 (E8C1, E8C2, E8C12, and E8C20) were generated with the gRNA targeting exon 8. To disrupt the VPS29 gene, three plasmids encoding VPS29 gene-targeting gRNAs were mixed (5′-GGACATCAAGTTATTCCATG-3′, 5′-GGACATCAAGTTATTCCATG-3′, and 5′-GGCAAACTGTTGCACCGGTG-3′) with the puromycin resistance–encoding plasmid, and clones were isolated as described above. The loss of VPS29 in these cells was tested by Western blotting against endogenous VPS29 protein. For the disruption of the endogenous CI-MPR gene, three px330 plasmids targeting distinct exons of CI-MPR (gRNA sequences were 5′-GCTTGTCCTGAGTTACGTGA-3′, 5′-GTGTGCACTACTTTGAGTGG-3′, and 5′-GAGAAGGAAGACCTCCTCTG-3′) were pooled and cotransfected with a GFP-tagged puromycin selection marker followed by clonal selection and Western blot–based testing of CI-MPR–null cells.

CRISPR-Cas9–mediated targeting of the retrograde sorting motif

To disrupt the WLM motif within the cytoplasmic tail of endogenous CI-MPR, HeLa cells were transfected with a px330 plasmid expressing a gRNA with the targeting sequence 5′-GAATGAAACAGAGTGGCTGA-3′, which cuts within the bases coding for W and L of the WLM motif as depicted in Fig. S4 G. After puromycin selection and clonal selection of transfected cells through limited dilution, 40 clonal cells were analyzed for retrograde sorting defects of CI-MPR. Most of the clonal cells had completely lost all CI-MPR expression, and genomic sequencing of several of these clones revealed that any frameshifting mutation within the CI-MPR tail at this position resulted in a complete loss of the protein (not depicted). Several clones displayed a partial loss of CI-MPR staining intensity and pronounced CI-MPR dispersal from the TGN, indicating retrograde sorting defects. Genomic sequencing of one of these clones revealed that one allele harbored a frameshifting mutation, which explained the partial loss of staining intensity. The other allele harbored the 18-bp deletion spanning the WLM motif shown in Fig. S4 G. This clone was then used for further experiments.

CRISPR-Cas9 screen

For the CRISPR screen, three px330 plasmids expressing gRNAs targeting distinct genomic regions of the gene to be targeted were mixed with a plasmid-encoding GFP-tagged puromycin resistance (pEGFP-C1 from Takara Bio Inc. with an N-terminally tagged puromycin *N*-acetyltransferase) in a ratio of 1:1:1:1 and then transfected into the HeLa cells using FuGENE HD. 1 d after transfection, transfected cells were selected with 3 µg/ml puromycin (Sigma-Aldrich) for 24 h, followed by recovery in regular growth medium for 3 d. The cells were then split onto coverslips and analyzed for a CI-MPR phenotype. Efficiency of the transfected CRISPR plasmids was verified by Western blotting of endogenous SNX1, SNX2, SNX5, and SNX6. After the screen, the most efficient SNX1/2/5/6-targeting CRISPR-Cas9 plasmids were chosen to generate clonal SNX1/2 and SNX5/6 double-KO cell lines with only one target site per gene. KO of the SNX-BAR proteins was confirmed by Western blotting. The respective gRNAs tar-

Downloaded from http://rupress.org/jcb/article-pdf/216/11/3677/1374505/jcb_201702137.pdf by guest on 26 August 2022

geting the individual genes were: SNX5 (5′-GCTCTGAAACGTGGG CAGTG-3′, 5′-GGTATGTCAATCTGAAGCGA-3′, and 5′-GCAGGA GGAGGACCGCAGCA-3′), SNX6 (5′-GATGTGCTGCCACACGAC AC-3′, 5′-GATTATATTCCAAGAAGACA-3′, and 5′-GGAGTATCA TAACCGAGTTA-3′), GGA1 (5′-GGAACTTGCCCACTTCGTCG-3′, 5′-GAAGAGGGTGAATGCCATCG-3′, and 5′-GATGGAGCC GGAGACTCTGG-3′), GGA2 (5′-GATGTGCATGAACCACTGTG-3′, 5′-GGTGTCCAAGAGGGTCAGTG-3′, and 5′-GGAAGTGCG AAGCCATGTGA-3′), AP1B1 (5′-GCATGCAGTTGACCACATCG-3′, 5′-GTCCAGATTCTCACACAGTG-3′, and 5′-GCTCGACCTCAT CCAGACCA-3′), AP1G1 (5′-GGAGGACTACAGATGTGTGG-3′, 5′-GGTATGCACCTTCCAAACGA-3′, and 5′-GTAAATGGGAATAAT ATCCG-3′), USP11 (5′-GGGCTCAAGAGAGGACATCG-3′, 5′-GTG GGCGAGAACGTCCACTG-3′, and 5′-GCACTGGTATAAGCAGTG GG-3′), WDR48 (5′-GTTGCAACCCAAATTGCAGG-3′, 5′-GTC ATTGTCATAATCTCCAG-3′, and 5′-GCATTGCTATTAAACAGA GA-3′), RAB7a (5′-GGGACACAGCAGGACAGGAA-3′, 5′-GGG AAGTTTTCAGGATCTCG-3′, and 5′-GAGCTGACTTTCTGACCA AGG-3′), Clathrin heavy chain (5′-GGTCAGCCTTAATTGCAGTG-3′, 5′-GTACTCCAGACACTATCCGT-3′, and 5′-GATCAGTGAAAA GCATGATG-3′), and SNX27 (5′-GCCCCTCACAGGAACGGAGG-3′, 5′-GGGTCTGGGCTCCACTGCGC-3′, and 5′-GTGCGGGGC CAAGTGAGCGA-3′). 1 wk after transfection of the respective CRI SPR plasmid mixes, efficiency of the KO in the mixed population of cells was tested by Western blotting for selected targets.

Cell culture and transfection

HEK-293, U2OS, HeLa, SHSY5Y, MDA-MB-231, and MCF-7 cells were grown in high-glucose DMEM (Sigma-Aldrich or Gibco) supplemented with 10% (vol/vol) FCS (Sigma-Aldrich) and penicillin-streptomycin (Gibco) and maintained in an incubator at 37°C and 5% CO_2. Cell lines were regularly tested for mycoplasma contamination. For siRNA transfection, Dharmafect-3 (GE Healthcare) was used for U2OS cells, whereas HiPerFect (QIAGEN) or Lipofectamine 2000 (Thermo Fisher Scientific) were used for HeLa cells. All siRNAs were made by GE Healthcare or MWG-Biotech. For DNA transfection, FuGENE 6 was used following the manufacturer's guidelines.

IPs by GFP trap

For GFP trap IPs from HEK293 cells, 20 µg of plasmid DNA containing GFP-tagged bait were transfected into 15-cm dishes using polyethylenimine (Polysciences) in a 1:3 ratio. 48 h after transfection, cells were lysed in 20 mM Tris-HCl, 50 mM NaCl, 5 mM $MgCl_2$, 0,5% NP-40, and EDTA-free protease inhibitor cocktail (Roche). After removing the cell debris, the lysates were incubated for 1 h with GFP-trap beads (ChromoTek) followed by 2× washing in lysis buffer.

Immunofluorescence

For immunofluorescence, cells were fixed with 4% PFA solution in PBS, permeabilized with 0.1% saponin, and blocked with 1% BSA in PBS before applying indicated primary antibodies and corresponding fluorescently labeled secondary antibodies. The secondary antibodies used in this study were all from Invitrogen (donkey anti–rabbit Alexa Fluor 488, donkey anti–mouse Alexa Fluor 594, goat anti–mouse Alexa Fluor 488, donkey anti–sheep Alexa Fluor 405, donkey anti–sheep Alexa Fluor 488, and donkey anti–rabbit Alexa Fluor 594). All images were acquired with a TCS 8ST-WS confocal microscope (Leica Microsystems). Images were analyzed and exported with the Volocity software package (PerkinElmer). The Pearson's correlation between the respective channels was quantified with the colocalization tool of the Volocity software after setting of uniform thresholds across conditions. The colocalization coefficient corresponds to the Manders's coefficient M2 calculated by the Volocity software after applying uniform thresholds across conditions.

Microscope image acquisition

All microscopy samples were embedded in homemade mowiol (Sigma-Aldrich) mounting medium, and images were acquired on an SP8 laser-scanning microscope (Leica Microsystems) equipped with STED depletion lasers. All images besides the STED superresolution images were acquired at room temperature with a 63× oil immersion objective (high-contrast Plan Apochromat 63× 1.40 NA Oil CS2) using the standard software (LAS X; Leica Microsystems) that came with the microscope. The LIF files were then opened with Volocity (PerkinElmer), exported as Bitmap files from Volocity, and transferred into Illustrator (Adobe) via cut and paste from Photoshop (Adobe). Where necessary for visibility in the final illustrator file, brightness was increased uniformly across the entire image and across all conditions shown using Photoshop.

STED microscopy

HeLa cells were fixed and stained as described under immunofluorescence. The high-resolution images of the Alexa Fluor 594 and the Alexa Fluor 488 channels were then acquired using the 100× oil immersion objective (high-contrast Plan Apochromat 100× 1.40 NA Oil STED WHITE) and the STED depletion lasers of an SP8 microscope at 95% power, beginning with the 594 channel to avoid excessive bleaching through the 488 depletion laser. The acquired images were then processed and exported using the Volocity image processing suite and as described in the previous section.

SILAC interactome analysis

GFP and the GFP–CI-MPR tail were lentivirally expressed in HEK293 cells, which were then grown in light, non-isotope–labeled R0K0 medium (for GFP) or in arginine 10– and lysine 8 (Silantes)–labeled heavy medium. For the SNX-BAR interactome, HEK293 cells were labeled in heavy medium (R10K8), and the GFP-tagged SNX-BARs were transfected into 15-cm dishes using polyethylenimine. GFP was transfected into nonlabeled HEK293 cells to serve as the control IPs. GFP-trap isolation and subsequent analysis has been described previously (Steinberg et al., 2012, 2013). In brief, 15-cm dishes of labeled cells expressing the indicated GFP-tagged proteins were lysed in 1 ml of complete lysis buffer (20 mM Tris-HCl, pH 7.8, 50 mM NaCl, 0.5% NP-40, and EDTA-free protease inhibitor cocktail). Lysates were centrifuged at top speed to remove debris and nuclei, and supernatant was incubated with 20 µl of GFP-trap beads (ChromoTek) for 30 min. The beads were then washed three times with 1 ml of lysis buffer, combined to one sample, and boiled in SDS sample buffer. After GFP-trap isolation and boiling, GFP and GFP–SNX-BAR (or CI-MPR tail) IPs were subjected to SDS-PAGE on commercial BOLT gradient gels (Invitrogen), Coomassie staining (Simply Blue; Invitrogen), and in-gel tryptic digest, and subsequent LC-MS/MS–based analysis was done on an Orbitrap (Thermo Fisher Scientific) mass spectrometer. The output was then analyzed using the MaxQuant software package (Max Planck Institute of Biochemistry). The original MaxQuant Output is shown in Tables S1 and S2.

Direct recombinant interaction studies

For all direct recombinant interaction studies, GST-tagged proteins were expressed as GST fusion proteins using pGEX-6p-3 (GE Healthcare) in *Escherichia coli* BL21 (New England Biolabs, Inc.). Expression was induced with 0.1 mM IPTG for 16 h in 18°C. Proteins were isolated from lysates made with PBS/1% Triton X-100 and lysed using sonication. The cell lysate was cleared using centrifugation and incu-

Downloaded from http://rupress.org/jcb/article-pdf/216/11/3677/1374505/jcb_201702137.pdf by guest on 26 August 2022

bated with glutathione Sepharose 4B beads (GE Healthcare) to pull down the proteins of interest. The His-tagged SNX-BAR proteins were produced using the pSecTag2 mammalian secretion system (Invitrogen). For that, SNX1, SNX2, SNX5, and SNX6 were cloned with a C-terminal His tag into the pSectag2 plasmid so that the pSecTag2 Igκ leader sequence ensures secretion of the proteins. Plasmids were either pooled as indicated in the figure or individually transfected into 15-cm dishes of HEK293 cells followed by 72 h incubation in full-growth DMEM. The beads with the GST-tagged bait constructs were then directly incubated with the filtered tissue culture supernatant and washed three times in 20 mM Tris, pH 7.8, 100 mM NaCl, 0.5% NP-40, and 0.1% BSA followed by boiling in sample buffer. One third of the beads was loaded onto a gel for the Coomassie-stained GST-input images, and two thirds were loaded onto a separate gel to detect His-tagged SNX-BAR proteins. To test whether the produced SNX-BAR proteins were glycosylated during export from the cells, small samples (30 µl) of the tissue culture supernatant were treated with 2 U of PNGaseF (Sigma-Aldrich) for 1 h followed by Western blot–based assessment of the apparent molecular weight compared with endogenous and untreated recombinant SNX-BARs. To produce SNX1 and SNX5 without (or with less) glycosylation, HEK293 cells were treated with 5 µg/ml tunicamycin (Santa Cruz Biotechnology, Inc.) over the 24-h medium collection period.

CI-MPR uptake assays

The respective HeLa cell lines were seeded onto glass coverslips and grown to 50–70% confluency in 12-well plates. Cells were then incubated with a mouse mAb against the extracellular domain of the CI-MPR (mouse anti-CD222; AbD Serotec) at 10 µg/ml in full-growth DMEM for 30 or 60 min at 37°C followed by washing in cold PBS and fixation in ice-cold 4% PFA in PBS. Cells were then permeabilized with 0.1% saponin, blocked with 1% BSA in PBS for 30 min, and stained with an antibody against TGN46 (sheep anti-TGN46; AbD Serotec) and also with an anti–mouse secondary antibody to visualize the internalized antibody.

RNAi

siRNA oligonucleotides were ordered from MWG-Biotec. The siRNA was transfected with Lipofectamine 2000 (Thermo Fisher Scientific) for HeLa cells or with Dharmafect-1 for U2OS cells. Cells were analyzed 72 h after transfection of the siRNA. The targeting sequences were SNX1, 5′-CCACGTGATCAAGTACCTT-3′; SNX2, 5′-GAUAGACCAGUUACAUCAA-3′; and VPS35, 5′-AAAUACCAGUUGACACUUA-3′.

Statistical analysis

To compare the effects of the respective treatments to the control cells, the *t* test function in Excel was used (two-tailed distribution; type 3). The number of independent repeat experiments is detailed in the respective figure legends. For the analysis of microscopy data (colocalization), each of the independent repeat experiments indicated in the figure legend contained at least five low-zoom images with multiple cells for each condition. For experiments with two independent repeats, the *t* test was performed across all individual images coming from the two independent experiments, and the total number or images is detailed in the figure legends. For experiments with at least three independent repeats, the *t* test was used to analyze significant differences in the averaged data from the three or more independent experiments. The distribution of the data was assumed to be normal, but this was not formally tested.

Online supplemental material

Fig. S1 shows CI-MPR antibody specificity, VPS35 rescue, and U2OS VPS35-KO clone information. Fig. S2 shows additional data on all HeLa VPS35-KO clones as well as on other tested cell lines. Fig. S3 shows how all clonal SNX-BAR double-KO cell lines display severe CI-MPR dispersal from the TGN. Fig. S4 shows how double knockdown of SNX1/2 results in CI-MPR dispersal. Fig. S5 shows all supplementary data on the IGF1R. Tables S1 and S2 show the original proteomics output for the CI-MPR tail interactome (Table S1) and for the SNX-BAR interactome (Table S2).

Acknowledgments

We would like to thank all members of the Life Imaging Center Freiburg, and especially Dr. Roland Nitschke and Dr. Angela Naumann, for their kind and competent technical support in all imaging-related things.

This study was funded by an Emmy Noether fellowship grant of the Deutsche Forschungsgemeinschaft (DFG STE2310/1-1) to F. Steinberg.

The authors declare no competing financial interests.

Author contributions: A. Kvainickas performed all biochemical work presented in the study. A. Jimenez-Orgaz performed the SNX-BAR rescue experiments and some of the CRISPR KOs. H. Nägele established KO cell lines and generated all the CRISPR-Cas9 targeting plasmids. Z. Hu and J. Dengjel performed the LC-MS/MS–based analysis for the SILAC experiments. F. Steinberg designed the study, performed most of the imaging work, and wrote the manuscript.

Submitted: 3 March 2017
Revised: 10 July 2017
Accepted: 1 August 2017

References

Arighi, C.N., L.M. Hartnell, R.C. Aguilar, C.R. Haft, and J.S. Bonifacino. 2004. Role of the mammalian retromer in sorting of the cation-independent mannose 6-phosphate receptor. *J. Cell Biol.* 165:123–133. http://dx.doi.org/10.1083/jcb.200312055

Burd, C., and P.J. Cullen. 2014. Retromer: a master conductor of endosome sorting. *Cold Spring Harb. Perspect. Biol.* 6:a016774. http://dx.doi.org/10.1101/cshperspect.a016774

Carlton, J., M. Bujny, B.J. Peter, V.M.J. Oorschot, A. Rutherford, H. Mellor, J. Klumperman, H.T. McMahon, and P.J. Cullen. 2004. Sorting nexin-1 mediates tubular endosome-to-TGN transport through coincidence sensing of high- curvature membranes and 3-phosphoinositides. *Curr. Biol.* 14:1791–1800. http://dx.doi.org/10.1016/j.cub.2004.09.077

Chen, D., H. Xiao, K. Zhang, B. Wang, Z. Gao, Y. Jian, X. Qi, J. Sun, L. Miao, and C. Yang. 2010. Retromer is required for apoptotic cell clearance by phagocytic receptor recycling. *Science.* 327:1261–1264. http://dx.doi.org/10.1126/science.1184840

Collins, B.M., S.J. Norwood, M.C. Kerr, D. Mahony, M.N.J. Seaman, R.D. Teasdale, and D.J. Owen. 2008. Structure of Vps26B and mapping of its interaction with the retromer protein complex. *Traffic.* 9:366–379. http://dx.doi.org/10.1111/j.1600-0854.2007.00688.x

Cong, L., F.A. Ran, D. Cox, S. Lin, R. Barretto, N. Habib, P.D. Hsu, X. Wu, W. Jiang, L.A. Marraffini, and F. Zhang. 2013. Multiplex genome engineering using CRISPR/Cas systems. *Science.* 339:819–823. http://dx.doi.org/10.1126/science.1231143

Derivery, E., C. Sousa, J.J. Gautier, B. Lombard, D. Loew, and A. Gautreau. 2009. The Arp2/3 activator WASH controls the fission of endosomes through a large multiprotein complex. *Dev. Cell.* 17:712–723. http://dx.doi.org/10.1016/j.devcel.2009.09.010

Dong, R., Y. Saheki, S. Swarup, L. Lucast, J.W. Harper, and P. De Camilli. 2016. Endosome-ER Contacts Control Actin Nucleation and Retromer Function through VAP-Dependent Regulation of PI4P. *Cell.* 166:408–423. http://dx.doi.org/10.1016/j.cell.2016.06.037

Dupont, J., and M. Holzenberger. 2003. Biology of insulin-like growth factors in development. *Birth Defects Res. C Embryo Today.* 69:257–271. http://dx.doi.org/10.1002/bdrc.10022

Elwell, C.A., N. Czudnochowski, J. von Dollen, J.R. Johnson, R. Nakagawa, K. Mirrashidi, N.J. Krogan, J.N. Engel, and O.S. Rosenberg. 2017. Chlamydia interfere with an interaction between the mannose-6-

Downloaded from http://rupress.org/jcb/article-pdf/216/11/3677/1374505/jcb_201702137.pdf by guest on 26 August 2022

phosphate receptor and sorting nexins to counteract host restriction. *eLife.* 6:e22709. http://dx.doi.org/10.7554/eLife.22709

Fjorback, A.W., M. Seaman, C. Gustafsen, A. Mehmedbasic, S. Gokool, C. Wu, D. Militz, V. Schmidt, P. Madsen, J.R. Nyengaard, et al. 2012. Retromer binds the FANSHY sorting motif in SorLA to regulate amyloid precursor protein sorting and processing. *J. Neurosci.* 32:1467–1480. http://dx.doi.org/10.1523/JNEUROSCI.2272-11.2012

Freeman, C.L., G. Hesketh, and M.N.J. Seaman. 2014. RME-8 coordinates the activity of the WASH complex with the function of the retromer SNX dimer to control endosomal tubulation. *J. Cell Sci.* 127:2053–2070. http://dx.doi.org/10.1242/jcs.144659

Gallon, M., and P.J. Cullen. 2015. Retromer and sorting nexins in endosomal sorting. *Biochem. Soc. Trans.* 43:33–47. http://dx.doi.org/10.1042/BST20140290

Gallon, M., T. Clairfeuille, F. Steinberg, C. Mas, R. Ghai, R.B. Sessions, R.D. Teasdale, B.M. Collins, and P.J. Cullen. 2014. A unique PDZ domain and arrestin-like fold interaction reveals mechanistic details of endocytic recycling by SNX27-retromer. *Proc. Natl. Acad. Sci. USA.* 111:E3604–E3613. http://dx.doi.org/10.1073/pnas.1410552111

García-de Lacoba, M., C. Alarcón, E.J. de la Rosa, and F. de Pablo. 1999. Insulin/insulin-like growth factor-I hybrid receptors with high affinity for insulin are developmentally regulated during neurogenesis. *Endocrinology.* 140:233–243. http://dx.doi.org/10.1210/endo.140.1.6393

Ghosh, P., J. Griffith, H.J. Geuze, and S. Kornfeld. 2003. Mammalian GGAs act together to sort mannose 6-phosphate receptors. *J. Cell Biol.* 163:755–766. http://dx.doi.org/10.1083/jcb.200308038

Gomez, T.S., and D.D. Billadeau. 2009. A FAM21-containing WASH complex regulates retromer-dependent sorting. *Dev. Cell.* 17:699–711. http://dx.doi.org/10.1016/j.devcel.2009.09.009

Griffin, C.T., J. Trejo, and T. Magnuson. 2005. Genetic evidence for a mammalian retromer complex containing sorting nexins 1 and 2. *Proc. Natl. Acad. Sci. USA.* 102:15173–15177. http://dx.doi.org/10.1073/pnas.0409558102

Haft, C.R., M. de la Luz Sierra, V.A. Barr, D.H. Haft, and S.I. Taylor. 1998. Identification of a family of sorting nexin molecules and characterization of their association with receptors. *Mol. Cell. Biol.* 18:7278–7287. http://dx.doi.org/10.1128/MCB.18.12.7278

Hao, Y.H., J.M. Doyle, S. Ramanathan, T.S. Gomez, D. Jia, M. Xu, Z.J.J. Chen, D.D. Billadeau, M.K. Rosen, and P.R. Potts. 2013. Regulation of WASH-dependent actin polymerization and protein trafficking by ubiquitination. *Cell.* 152:1051–1064. http://dx.doi.org/10.1016/j.cell.2013.01.051

Harrison, M.S., C.S. Hung, T.T. Liu, R. Christiano, T.C. Walther, and C.G. Burd. 2014. A mechanism for retromer endosomal coat complex assembly with cargo. *Proc. Natl. Acad. Sci. USA.* 111:267–272. http://dx.doi.org/10.1073/pnas.1316482111

Harterink, M., F. Port, M.J. Lorenowicz, I.J. McGough, M. Silhankova, M.C. Betist, J.R.T. van Weering, R.G.H.P. van Heesbeen, T.C. Middelkoop, K. Basler, et al. 2011. A SNX3-dependent retromer pathway mediates retrograde transport of the Wnt sorting receptor Wntless and is required for Wnt secretion. *Nat. Cell Biol.* 13:914–923. http://dx.doi.org/10.1038/ncb2281

Hierro, A., A.L. Rojas, R. Rojas, N. Murthy, G. Effantin, A.V. Kajava, A.C. Steven, J.S. Bonifacino, and J.H. Hurley. 2007. Functional architecture of the retromer cargo-recognition complex. *Nature.* 449:1063–1067. http://dx.doi.org/10.1038/nature06216

Kvainickas, A., A.J. Orgaz, H. Nägele, B. Diedrich, K.J. Heesom, J. Dengjel, P.J. Cullen, and F. Steinberg. 2017. Retromer- and WASH-dependent sorting of nutrient transporters requires a multivalent interaction network with ANKRD50. *J. Cell Sci.* 130:382–395. http://dx.doi.org/10.1242/jcs.196758

Lin, S.X., W.G. Mallet, A.Y. Huang, and F.R. Maxfield. 2004. Endocytosed cation-independent mannose 6-phosphate receptor traffics via the endocytic recycling compartment en route to the trans-Golgi network and a subpopulation of late endosomes. *Mol. Biol. Cell.* 15:721–733. http://dx.doi.org/10.1091/mbc.E03-07-0497

Lucas, M., D.C. Gershlick, A. Vidaurrazaga, A.L. Rojas, J.S. Bonifacino, and A. Hierro. 2016. Structural Mechanism for Cargo Recognition by the Retromer Complex. *Cell.* 167:1623–1635.

Ludwig, T., J. Eggenschwiler, P. Fisher, A.J. D'Ercole, M.L. Davenport, and A. Efstratiadis. 1996. Mouse mutants lacking the type 2 IGF receptor (IGF2R) are rescued from perinatal lethality in Igf2 and Igf1r null backgrounds. *Dev. Biol.* 177:517–535. http://dx.doi.org/10.1006/dbio.1996.0182

Meyer, C., D. Zizioli, S. Lausmann, E.L. Eskelinen, J. Hamann, P. Saftig, K. von Figura, and P. Schu. 2000. mu1A-adaptin-deficient mice: lethality, loss of AP-1 binding and rerouting of mannose 6-phosphate receptors. *EMBO J.* 19:2193–2203. http://dx.doi.org/10.1093/emboj/19.10.2193

Peralta, E.R., B.C. Martin, and A.L. Edinger. 2010. Differential effects of TBC1D15 and mammalian Vps39 on Rab7 activation state, lysosomal morphology, and growth factor dependence. *J. Biol. Chem.* 285:16814–16821. http://dx.doi.org/10.1074/jbc.M110.111633

Popoff, V., G.A. Mardones, S.-K. Bai, V. Chambon, D. Tenza, P.V. Burgos, A. Shi, P. Benaroch, S. Urbé, C. Lamaze, et al. 2009. Analysis of articulation between clathrin and retromer in retrograde sorting on early endosomes. *Traffic.* 10:1868–1880. http://dx.doi.org/10.1111/j.1600-0854.2009.00993.x

Robinson, M.S., D.A. Sahlender, and S.D. Foster. 2010. Rapid inactivation of proteins by rapamycin-induced rerouting to mitochondria. *Dev. Cell.* 18:324–331. http://dx.doi.org/10.1016/j.devcel.2009.12.015

Rojas, R., S. Kametaka, C.R. Haft, and J.S. Bonifacino. 2007. Interchangeable but essential functions of SNX1 and SNX2 in the association of retromer with endosomes and the trafficking of mannose 6-phosphate receptors. *Mol. Cell. Biol.* 27:1112–1124. http://dx.doi.org/10.1128/MCB.00156-06

Roquemore, E.P., and G. Banting. 1998. Efficient trafficking of TGN38 from the endosome to the trans-Golgi network requires a free hydroxyl group at position 331 in the cytosolic domain. *Mol. Biol. Cell.* 9:2125–2144. http://dx.doi.org/10.1091/mbc.9.8.2125

Seaman, M.N.J. 2004. Cargo-selective endosomal sorting for retrieval to the Golgi requires retromer. *J. Cell Biol.* 165:111–122. http://dx.doi.org/10.1083/jcb.200312034

Seaman, M.N.J. 2007. Identification of a novel conserved sorting motif required for retromer-mediated endosome-to-TGN retrieval. *J. Cell Sci.* 120:2378–2389. http://dx.doi.org/10.1242/jcs.009654

Seaman, M.N.J., J.M. McCaffery, and S.D. Emr. 1998. A membrane coat complex essential for endosome-to-Golgi retrograde transport in yeast. *J. Cell Biol.* 142:665–681. http://dx.doi.org/10.1083/jcb.142.3.665

Seaman, M.N.J., M.E. Harbour, D. Tattersall, E. Read, and N. Bright. 2009. Membrane recruitment of the cargo-selective retromer subcomplex is catalysed by the small GTPase Rab7 and inhibited by the Rab-GAP TBC1D5. *J. Cell Sci.* 122:2371–2382. http://dx.doi.org/10.1242/jcs.048686

Shi, A., L. Sun, R. Banerjee, M. Tobin, Y. Zhang, and B.D. Grant. 2009. Regulation of endosomal clathrin and retromer-mediated endosome to Golgi retrograde transport by the J-domain protein RME-8. *EMBO J.* 28:3290–3302. http://dx.doi.org/10.1038/emboj.2009.272

Shi, H., R. Rojas, J.S. Bonifacino, and J.H. Hurley. 2006. The retromer subunit Vps26 has an arrestin fold and binds Vps35 through its C-terminal domain. *Nat. Struct. Mol. Biol.* 13:540–548. http://dx.doi.org/10.1038/nsmb1103

Steinberg, F., K.J. Heesom, M.D. Bass, and P.J. Cullen. 2012. SNX17 protects integrins from degradation by sorting between lysosomal and recycling pathways. *J. Cell Biol.* 197:219–230. http://dx.doi.org/10.1083/jcb.201111121

Steinberg, F., M. Gallon, M. Winfield, E.C. Thomas, A.J. Bell, K.J. Heesom, J.M. Tavaré, and P.J. Cullen. 2013. *Nat. Cell Biol.* 15:461–471. http://dx.doi.org/10.1038/ncb2721

Strochlic, T.I., T.G. Setty, A. Sitaram, and C.G. Burd. 2007. Grd19/Snx3p functions as a cargo-specific adapter for retromer-dependent endocytic recycling. *J. Cell Biol.* 177:115–125. http://dx.doi.org/10.1083/jcb.200609161

van Weering, J.R.T., R.B. Sessions, C.J. Traer, D.P. Kloer, V.K. Bhatia, D. Stamou, S.R. Carlsson, J.H. Hurley, and P.J. Cullen. 2012. Molecular basis for SNX-BAR-mediated assembly of distinct endosomal sorting tubules. *EMBO J.* 31:4466–4480. http://dx.doi.org/10.1038/emboj.2012.283

Varandas, K.C., R. Irannejad, and M. von Zastrow. 2016. Retromer Endosome Exit Domains Serve Multiple Trafficking Destinations and Regulate Local G Protein Activation by GPCRs. *Curr. Biol.* 26:3129–3142. http://dx.doi.org/10.1016/j.cub.2016.09.052

Vilariño-Güell, C., C. Wider, O.A. Ross, J.C. Dachsel, J.M. Kachergus, S.J. Lincoln, A.I. Soto-Ortolaza, S.A. Cobb, G.J. Wilhoite, J.A. Bacon, et al. 2011. VPS35 mutations in Parkinson disease. *Am. J. Hum. Genet.* 89:162–167. http://dx.doi.org/10.1016/j.ajhg.2011.06.001

Wassmer, T., N. Attar, M.V. Bujny, J. Oakley, C.J. Traer, and P.J. Cullen. 2007. A loss-of-function screen reveals SNX5 and SNX6 as potential components of the mammalian retromer. *J. Cell Sci.* 120:45–54. http://dx.doi.org/10.1242/jcs.03302

Wassmer, T., N. Attar, M. Harterink, J.R.T. van Weering, C.J. Traer, J. Oakley, B. Goud, D.J. Stephens, P. Verkade, H.C. Korswagen, and P.J. Cullen. 2009. The retromer coat complex coordinates endosomal sorting and dynein-mediated transport, with carrier recognition by the trans-Golgi network. *Dev. Cell.* 17:110–122. http://dx.doi.org/10.1016/j.devcel.2009.04.016

Wong, M., and S. Munro. 2014. The specificity of vesicle traffic to the Golgi is encoded in the golgin coiled-coil proteins. *Science.* 346:1256898. http://dx.doi.org/10.1126/science.1256898

Downloaded from http://rupress.org/jcb/article-pdf/216/11/3677/1374505/jcb_201702137.pdf by guest on 26 August 2022

Zhang, X.M., B. Walsh, C.A. Mitchell, and T. Rowe. 2005. TBC domain family, member 15 is a novel mammalian Rab GTPase-activating protein with substrate preference for Rab7. *Biochem. Biophys. Res. Commun.* 335:154–161. http://dx.doi.org/10.1016/j.bbrc.2005.07.070

Zhong, Q., C.S. Lazar, H. Tronchère, T. Sato, T. Meerloo, M. Yeo, Z. Songyang, S.D. Emr, and G.N. Gill. 2002. Endosomal localization and function of sorting nexin 1. *Proc. Natl. Acad. Sci. USA*. 99:6767–6772. http://dx.doi.org/10.1073/pnas.092142699

Zimprich, A., A. Benet-Pagès, W. Struhal, E. Graf, S.H. Eck, M.N. Offman, D. Haubenberger, S. Spielberger, E.C. Schulte, P. Lichtner, et al. 2011. A mutation in VPS35, encoding a subunit of the retromer complex, causes late-onset Parkinson disease. *Am. J. Hum. Genet.* 89:168–175. http://dx.doi.org/10.1016/j.ajhg.2011.06.008

Downloaded from http://rupress.org/jcb/article-pdf/216/11/3677/1374505/jcb_201702137.pdf by guest on 26 August 2022